Mutation of the 3-phosphoinositide-dependent protein kinase-1 (PDK1) substrate-docking site in the developing brain causes microcephaly with abnormal brain morphogenesis independently of Akt, leading to impaired cognition and disruptive behaviors.

Lluís Cordón-Barris[a]*, Sònia Pascual-Guiral[a], Shaobin Yang[a], Lydia Giménez-Llort[b], Silvia Lope-Piedrafita[c], Carlota Niemeyer[a], Enrique Claro[a], Jose M Lizcano[a] & Jose R Bayascas[a#]

Institut de Neurociències & Departament de Bioquímica i Biologia Molecular, Universitat Autònoma de Barcelona, Barcelona, Spain[a]; Institut de Neurociències & Departament de Psiquiatria i Medicina Legal, Universitat Autònoma de Barcelona, Barcelona, Spain[b]; Servei de Ressonància Magnètica Nuclear, Universitat Autònoma de Barcelona, Barcelona, Spain and Centro de Investigación Biomédica en Red en Bioingeniería, Biomateriales y Nanomedicina (CIBER-BBN)[c]

Running Head: Role of PDK1 in neurodevelopment behavior disorders

#Address correspondence to Jose R Bayascas, joseramon.bayascas@uab.cat

*Present address: GIGA-Neurosciences, Université de Liège, Liège, Belgium

"This is the Accepted Manuscript of an article published in "Molecular and Cellular Biology", vol. 36, no. 23 (December 2016), p.2967-2982.

DOI: 10.1128/MCB.00230-16. Available at: http://dx.doi.org/10.1128/MCB.00230-16"

Number of words for Abstract: 175; Material and Methods: 2238; combined word count for the Introduction, Results, and Discussion: 5174. Length of the text (excluding spaces) for the Abstract, Introduction, Results, Discussion, and Figure Legends: 39298

Abstract.

The phosphoinositide 3-kinase (PI 3-kinase)/Akt signaling pathway plays essential roles during neuronal development. The 3-phosphoinositide-dependent protein kinase 1 (PDK1) coordinates the PI 3-kinase signals by activating twenty three kinases of the AGC family including Akt. Phosphorylation of a conserved docking site in the substrate is a requisite for PDK1 to recognize, phosphorylate and activate most of these kinases, with the exception of Akt. We exploited this differential mechanism of regulation by generating neuronal-specific conditional knock-in mice expressing the mutant form of PDK1 L155E in which the substrate-docking site binding motif, termed the PIF-pocket, was disrupted. As a consequence, activation of all the PDK1 substrates tested excluding Akt was abolished. Mice exhibited microcephaly, altered cortical layering and reduced circuitry, leading to cognitive deficits and exacerbated disruptive behavior combined with diminished motivation. The abnormal patterning of the adult brain arise from the reduced ability of the embryonic neurons to polarize and extend their axons, therefore highlighting the essential roles that the PDK1 signaling beyond Akt plays in mediating the neuronal responses that are instructive for brain development.

Introduction.

The phosphoinositide 3-kinase (PI 3-kinase) signaling pathway regulates cell survival, proliferation, growth, motility as well as metabolism in response to extracellular signals. Class I PI 3-kinases phosphorylate the membrane phospholipid phosphatidylinositol-4,5-bisphosphate (PtdIns(4,5)P_2) to generate the phosphatidylinositol-3,4,5-trisphosphate (PtdIns(3,4,5)P_3) second messenger (1,2). In neurons, stimulation of PI 3-kinase by neurotrophic factors, neurotransmitters or guidance cues results in the activation of the Protein Kinase B (PKB, also termed Akt), the most studied downstream effector of this signaling pathway. Akt phosphorylates and inactivates a number of cellular substrates controlling different aspects of neuronal development. These include PRAS40 and TSC2, leading to mTORC1 activation, which in turns promotes the synthesis of selected sets of proteins involved in the differentiation program (3); GSK3, which regulate cytoskeleton dynamics and participate in the establishment and maintenance of neuronal polarity (4,5); and FOXO, that promote the expression of genes inhibiting apoptosis (6). Genetic analysis in mice has uncovered the functional significance of PI 3-kinase for brain morphology and physiology (7-10), whereas deregulation of this signaling pathway has pathophysiological consequences in human neurodevelopmental disorders such as schizophrenia (11-13) and autism (14,15).

The 3-phosphoinositide-dependent protein kinase-1 transduces many agonist-induced cellular responses by activating an entire set of AGC kinase-family members in addition to Akt (16). These include S6K, SGK, RSK and PKC isoforms. Upon cell stimulation, PDK1 is enabled to phosphorylate the T-loop of all these AGC kinases, resulting in their activation (17,18).

Since PDK1 is constitutively active in cells, the previous phosphorylation of a second activating residue located in a C-terminal conserved hydrophobic motif becomes rate limiting for PDK1 to bind and activate most substrates. The phosphorylated hydrophobic motif acts in this manner as a substrate-docking site recognized by a small groove within the PDK1 catalytic domain termed PIF-pocket (19,20). By contrast, phosphorylation of Akt at the hydrophobic motif is not required for PDK1 to activate this kinase. The exclusive presence in both PDK1 and Akt of pleckstrin homology (PH) domains able to specifically interact with PtdIns(3,4,5)P_3 results in their co-localization at the plasma membrane, where PDK1 can phosphorylate and activate Akt (16).

The final demonstration that these two mechanisms operates in vivo came from the analysis of two single-aminoacid, rationally designed PDK1 mutations abrogating the function of either the PH-domain or the PIF-pocket motif (21). We recently reported how in the $PDK1^{K465E/K465E}$ knock-in mice, which express a mutant form of PDK1 incapable of phosphoinositide binding, activation of Akt was selectively affected. As a consequence, the ability of hippocampal and cortical embryonic neurons to differentiate was markedly impaired (22).

Full knock-in mice expressing a mutant form of PDK1 in which the Leucine residue at position 155 within the PIF-pocket was replaced by Glutamic acid (L155E) were previously generated, which died at mid gestation. In the $PDK1^{L155E/L155E}$ mice, activation of all the PDK1-regulated substrates with the exception of Akt was totally abolished (23). To define the contribution of the PDK1 signaling beyond Akt to neurodevelopmental regulation, here we targeted the expression of the PDK1 L155E mutant protein to the developing brain. The PDK1 mutant mice were microcephalic, with neuronal polarization and axonal elongation significantly inhibited in the mutant neurons. As a consequence, the patterning of the brain

was dramatically perturbed, as denoted by cortical layering alterations and reduced circuitry. These resulted in impaired cognition along with abnormal behaviors, which further highlights the importance of PDK1 targets different from Akt in mediating signaling responses that are key to brain development.

Materials and methods

Mice

The Nestin-Cre transgenic mice were kindly provided by Professor Ulrich Mueller at the Scripps Research Institute (24), whereas the PDK1 L155E conditional knock-in mice and the genotyping procedures were previously described (25). Animal maintenance conditions and experimental research was performed in accordance with 2010/63/UE regarding the care and use of animals for experimental procedures. The study complies with the ARRIVE guidelines developed by the NC3Rs (26).

Primary cultures

Neuronal primary cultures were established from E15,5 embryos as previously described (22). Cortical cells were plated at a density of $20x10^4$ cells/ml on 50 µg/ml of poly-D-Lysine- coated plates and maintained for six days in vitro (DIV) before treatments**,** whereas hippocampal cells were plated at a density of $7.5x10^4$ cells/ml onto 12-mm glass coverslips coated with 150 µg/ml poly-D-Lysine placed in 24-well plates for four days in vitro.

MRI analysis

Adult mice were terminated, brains dissected and right hemispheres kept at - 80ºC for biochemical analysis. Left hemispheres were fixed for 2 hours in 4% paraformaldehyde, preserved in 70% ethanol solution at 4ºC and embedded in 1,5% agarose in PBS. 1H-Magnetic resonance imaging studies were performed in a 7T Bruker BioSpec 70/30 USR spectrometer equipped with a mini-imaging gradient set (400mT/m), a 72 mm inner diameter circular polarized linear transmitter volume coil and a received-only mouse head surface coil. Images were acquired using a multislice fast low angle shot (FLASH) sequence from the Bruker Paravision® 5.1 library (repetition time = 450ms, echo time =

5.4ms, excitation flip angle = 40º) in 33 contiguous slices with 0.5 mm thickness, an acquisition matrix of 256×256, and a field of view 19.2mm×19.2mm, giving a voxel resolution of 0.0028125mm^3. Imaging data were Fourier transformed in ParaVision, and then visualized using the ImageJ software.

Determination of organ volume and cell size

Organ volume was determined using the Cavalieri method (27) applied to either MRI datasheets of the adult brain or physical sections of embryonic brain samples. MRI images were displayed on ImageJ, outlined and the total number of pixels multiplied by the voxel resolution and by a factor of 2 to obtain the adult brain volume, which was assumed as twice the volume of one hemisphere. Embryonic brain paraffin sections of 5 µm were collected at systematically spaced locations (k=96 µm) from a random starting position and photographed with a Nikon SMZ800 stereomicroscope at 1X magnification using a digital camera. A square lattice grid of 0.9149 mm^2 (d^2) was then overlaid on the picture using the program Photoshop version vCS5.1 and the number of intersections (P) hitting either the whole head or the brain scored. The volume was estimated by using the equation $\sum P \times d^2 \times k$. The number and size of the cells was determined on E15.5 dissociated cortex tissues with the ScepterTM 2.0 Handheld Automated Cell Counter (Millipore).

Evaluation of neuronal proliferation, apoptosis and survival

For the survival studies, cortical neurons obtained at E15,5 were cultured in complete Neurobasal media supplemented with B27 for six days in vitro, washed twice with DMEM without serum and then either re-incubated in conditioned media or trophic deprived for 24 hours in serum-free Neurobasal medium in the absence or presence of 50 ng/ml of BDNF (Brain derived neurotrophic factor; Alomone). Cell viability was determined by the MTT

(3-(4,5-dimethylthiazol-2-yl)-2,5-diphenyltetrazolium bromide) reduction assay, whereas the percentage of apoptosis was determined upon Hoechst staining by scoring the number of cells with fragmented or condensed nuclei, as described (22). For the proliferation and apoptosis studies, E15,5 cortical neurons were cultured in complete Neurobasal media supplemented with B27 for the indicated days in vitro and then processed for immunocytochemistry with antibodies recognizing the Ki67 proliferation marker and the active caspase-3 apoptotic marker.

Immunocytochemistry

Cells were fixed in 4% paraformaldehyde in PBS for 20 min at room temperature, rinsed twice with PBS, permeabilized with 0.02% saponin diluted in PBS for 7 min at room temperature and blocked with 5% BSA, 0.01% saponin, 10 mM glycine in PBS for 1 h at room temperature. Primary antibodies diluted in PBS with 0.01% saponin and 1% normal goat serum were incubated overnight at 4ºC. Cells were then incubated with the appropriate secondary antibodies diluted 1:400 in the same solution for 90 min and counterstained with 1µg/ml of Hoechst 33342 for 30 min. Coverslips were mounted onto microscope slides with FluorSave Reagent.

Evaluation of differentiation

Hippocampal cells fixed at different days in vitro were immunostained with the dendritic marker MAP2, the axonal marker Tau1 and counterstained with 1 µg/ml of the nuclear dye Hoechst 33342. Images for the green, red and blue channels were taken simultaneously with an epifluorescence microscope (Nikon Eclipse 90i) interfaced to a DXM 1200F camera at a 20X magnification. The number and length of axons, dendrites, dendritic branches and the soma diameter were measured with the NeuronJ plugin and scored with the Cell counter from ImageJ 1.42q (Wayne Rasband, National Institutes of Health).

Generation of protein extracts and western blot analysis

E15,5 cortical neurons cultured for six days in vitro in complete Neurobasal media supplemented with B27 were starved for 4 h in Neurobasal without B27 and subsequently stimulated with 50 ng/ml BDNF for 15 minutes. Cells were scrapped from wells in ice-cold Lysis Buffer (50 mM Tris-HCl pH 7.5, 1 mM EGTA, 1 mM EDTA, 1 mM sodium orthovanadate, 50 mM sodium fluoride, 5 mM sodium pyrophosphate, 10 mM sodium-glycerophosphate, 0.27 M sucrose, 1% w/v Triton X-100, 0.1% v/v 2-mercaptoethanol, and a 1:100 dilution of protease inhibitor cocktail, Sigma). Tissue extracts were prepared by homogenizing on ice the frozen tissue in a 10-fold volume excess of ice-cold Lysis Buffer using the Polytron. Lysates were centrifuged at 4°C for 10 min at 13.000 rpm and supernatants aliquoted and preserved at -20°C. Protein concentrations were determined by the Bradford method using bovine serum albumin as a standard. The activation state of the different pathways was assessed by immunoblotting the extracts (10 µg) with the indicated antibodies, which were detected with the appropriate horseradish peroxidase-conjugated secondary antibodies. Membranes were incubated with the enhanced chemiluminescence reagent (ECL), then either exposed to Super RX Fujifilm and developed, or detected using a ChemiDoc MP Imaging System (Biorad), and then quantified by using the ImageJ software.

Affinity purification of PDK1.

10 µl of Streptavidin-Sepharose (GE Heathcare) was conjugated to 0.5 µg of biotinylated PIF peptide (Biotin-C6 spacer-REPRILSEEEQEMFRDFAYIADWC) and incubated with 0.3 mg of pre-cleared tissue lysates at 4 ºC overnight on a shaking platform. The pull-downs were washed twice with 1 ml of Lysis Buffer supplemented with 150 mM NaCl, resuspended in Sample Loading Buffer, electrophoresed and then immunoblotted for PDK1.

Antibodies.

The Akt and PRAS40 total antibodies were kindly provided by Dario Alessi from the University of Dundee. The PDK1 (#3062), TrkB Tyr706/707-P (#4621), TrkB (#4603), Akt Thr308-P (#4056), Akt Ser473-P (#4060), PRAS40 Thr246-P (#2997), pan-PDK1 site PKCγ Thr514-P antibody (#9379), S6K Thr389-P (#9234), S6K (#9202), S6 protein Ser235/236-P (#4858), S6 protein (#2217), ERK1/2 (#9102), RSK Ser380-P (#9335) and RSK 1/2/3 (#9355) antibodies were purchased from Cell Signaling Technology. The RSK Ser227-P (#12445) antibody was obtained from Santa Cruz Biotechnology, the SGK1 antibody (#S5188) from Sigma, and the PKCα antibody (#P16520) from Transduction Laboratories. Secondary antibodies were from Pierce.

For immunofluorescence experiments we used the Tau-1 (#MAB3420), the GAD67 (#MAB5406), the Parvoalbumin (#MAB1572) and the NeuN (#MAB377) antibodies from Millipore, the pan-axonal neurofilament (#SMI-312R) antibody from Covance, the rabbit MAP2 (#M3696) antibody from Sigma, the CUX1 (#13024) antibody from Santa Cruz Biotechnology, the Ki67 (#ab156956) and the Doublecortin (#ab18723) antibodies from Abcam, and the Caspase-3 cleaved (#9661) antibody from Cell Signaling. Alexa Fluor 594-conjugated goat anti-rabbit (#A11072), Alexa Fluor 488-conjugated goat anti-mouse (#A11017) and Alexa Fluor 594-conjugated goat anti-rat (#A11007) secondary antibodies were obtained from Molecular Probes (Life Technologies).

Immunohistochemistry

Adult mice were intraperitoneally anesthetized with 0.4 mg/g body weight of pentobarbital, then an intracardiac injection of 70 heparin units was administered before perfusion with 0.9% NaCl followed by 4% buffered paraformaldehyde. Brains were extracted, post-fixed for 2 hours in 4% paraformaldehyde and preserved in 70% ethanol solution at 4ºC.

Embryos were dissected from E15,5 plug-tested pregnant females, decapitated, the whole head fixed for 2 hours in 4% paraformaldehyde and then preserved in 70% ethanol solution at 4ºC. In both cases, samples from three littermates of different genotype were embedded in the same paraffin block, with a final number of blocks of three, which were then sliced into 5µm thick coronal sections with a Leica RM2255 microtome. Sections were dry-heated for 2 hours at 60ºC, rehydrated, boiled 10 min in 10 mM sodium citrate pH 6 for antigen retrieval, cooled down for 30 min on ice and washed three times with Tris-buffered saline (TBS; 25 mM Tris pH7.5, 150 mM NaCl). Samples were blocked in TBS containing 0.02% Triton and 5% goat serum for 30 min and incubated overnight at 4°C with primary antibodies diluted in the same blocking solution. Sections were rinsed with TBS buffer, incubated for 1,5 hours at room temperature with the corresponding secondary antibodies diluted 1:400 in TBS and counterstained with 1 µg/ml Hoechst 33342 before mounting in Fluorsave reagent. Immunostained sections were photographed with a Nikon Eclipse 90i epifluorescence microscope, and the captured images were processed and analyzed with ImageJ 1.42q (Wayne Rasband, National Institutes of Health) and Fiji (http://pacific.mpi-cbg.de/wiki/index.php/Main_Page) software.

Behavioral Analysis

A sample of six PDK1$^{fl/fl}$ CRE^{+} mutant and six PDK1$^{fl/fl}$ CRE^{-} matched controls twelve-months old female mice were confronted to a standardized battery of behavioral tests (28,29) administered during 10 consecutive days, as a preliminary screening of the behavioral phenotypes of the mutant mice. On day 1, observation of undisturbed behavior in the homecage including sociability, barbering and sleeping in groups pattern, was immediately followed by the assessment of several sensorimotor tasks. Motor coordination and equilibrium were assessed in the wood and rod tests, by the distance covered and the

latency to fall off a horizontal 1.3 cm-wide wooden rod and a 1 cm-diameter wire rod on two consecutive 20 s trials. Prehensility and motor coordination were measured as the distance covered on the wire hang test, where the animals were allowed to cling with its forepaws for two trials of 5 s and a third 60 s trial. Muscle strength was measured as the time until falling off the wire in the 60 s trial. Nesting behavior using paper towel was measured in isolation (housing condition on day 10), according to Deacon's 5-point scale (30). The secondary and tertiary screen address neuropsychiatric-like deficits by assessing spontaneous exploratory behavior, anxiety-like behaviors, circadian activity and cognition in a series of test involving different degrees of complexity. Neophobia in the corner test was recorded on day 2**,** in a new home-cage by the horizontal (n of visited corners) and vertical (n and latency of rearings) activity during a period of 30s. Immediately after, exploratory activity and anxiety-like behaviors in a standard open-field test were measured for 10 min. Horizontal (cm) and vertical (rearings) locomotor activities were recorded for each minute of the test. The following items of behavior were recorded: Freezing (latency of initial movement), thigmotaxis (latency of leaving the central square and that of entering in the peripheral ring 10 cm to the walls), and self-grooming behavior (latency, number and duration of groomings). Defecation and urination were also measured. On day 3, marble-burying test was performed in standard cages containing 10 glass marbles (1x1x1 cm) evenly spaced on a 5 cm thick layer of sawdust. Latency to contact a piece of marble was measured and at the end of the 30-min test, the number of marbles was counted as follows: Intact (number of marbles unmanipulated), Change position (the number of marbles at least ½ buried by sawdust and change rotated 90º or 180º) and Buried (the number of marbles 100% buried by sawdust) (30). On the next three days (days 4-6)**,** the perceptual visual learning and spatial learning and memory were assessed in a 3-days water maze. Animals

were trained to criterion (90% escaping in under 60 s) in a series of cued visible platform trials (7 cm diameter, 1 cm above the water surface, position indicated by a visible 5 x 8 cm striped flag, 20 min inter-trial time) in a pool (Intex Recreation Corp. CA, USA; 91 cm diameter, 40 cm deep, 25ºC opaque water). This required four platform trials (CUE1–CUE4). The last visible platform trial of any animal is considered to be its post-habituation baseline, and is designated CUE4 (cued visible platform trial 4). Mice that failed to find the platform within 60 s were manually guided to the platform and placed on it for 5–10 s, the same period as successful animals. 24 h after the last cued platform trial, the animals were tested in a series of four hidden platform trials (PT1–PT4, 20 min apart). In these place-learning task, the hidden platform (1.5 cm below the water surface) was located in a new position, reversal to the one used for cue-learning. Escape latencies were measured with a stop-watch. Episodes of immobility (flotation) were measured. On days 7-10, circadian motor activity was tested for 84 consecutive hours in a home cage equipped with a running wheel (31).

Statistical analysis

Two-way analysis of variance and Student's t test analysis were applied to compare differences among categories, where * indicates $P < 0.05$ and ** $P < 0.005$ compared to controls as depicted in the figures. Data analysis was done using the GraphPad Prism software (GraphPad Software, La Jolla, CA, USA).

Results

Generation of neuronal-specific PDK1 L155E knock-in mice.

We followed the minigene conditional knock-in approach to limit the expression of the PDK1 mutant protein to the neuronal lineage (25). In this method, a conditional allele was constructed in which the wild type protein is expressed from the endogenous locus through the first two PDK1 exons, whereas expression of the remaining coding region occurs through a LoxP site-flanked minigene DNA cassette consisting on the wild type PDK1 open reading frame from exons 3 to 14 followed by the natural transcriptional termination and polyadenylation signals. The construct is designed so that upon CRE-Recombinase mediated excision of the floxed minigene, a mutated version of exon 4 coding for glutamic acid at position 155 of the mouse PDK1 protein will be transcribed (Fig. 1A).

A potential drawback of this floxed allele is its reported inability to efficiently use the termination signals of the minigene cassette to finish transcription, which continued into the knock-in region of the gene even in the absence of CRE and produced significant amounts of mRNA for mutant PDK1 (25). However, we reasoned that this attribute, upon the appropriate genetic crosses, would give rise to a valuable allelic series with increasing expression of the mutant PDK1 protein. Hence, mice homozygous for the PDK1 conditional transgen were crossed with Nestin-CRE mice, which express the CRE-Recombinase under the control of the neuron-specific enhancer of the nestin promoter in precursors of both neurons and glia starting at embryonic day E10.5 (24). The PDK1 L155E conditional floxed allele will be referred as $PDK1^{fl}$ through the text for simplicity. The $PDK1^{fl/fl}$ CRE^{+} mice, but not the $PDK1^{+/fl}$ CRE^{-}, $PDK1^{+/fl}$ CRE^{+} or $PDK1^{fl/fl}$ CRE^{-} mice, were born at a reduced Mendelian distribution (Fig. 1B). We confirmed that the

PDK1 protein was expressed at similar levels in samples of the different genotypes analyzed (Fig. 1C). We next incubated protein extracts from either brain or liver with Sepharose conjugated to PIF-tide, a synthetic polypeptide corresponding to the aminoacid sequence of the PDK1 substrate-docking site. The PIF-tide interacts strongly with the PIF-pocket of wild type PDK1 but cannot interact with the PDK1 L155E mutant protein (32,33). PDK1 could be affinity-purified with high efficiency from $PDK1^{+/fl}$ CRE^{-}, $PDK1^{+/fl}$ CRE^{+} and, to a lesser extent, from $PDK1^{fl/fl}$ CRE^{-} brain extracts, but not from the $PDK1^{fl/fl}$ CRE^{+} mutant mice brain extracts, thereby biochemically confirming the expected gradation in the expression of the mutant PDK1 L155E protein rather than the wild type one. As a control, we demonstrated that in the liver tissues, which does not express CRE, PDK1 could be affinity-purified with the same reduced efficiency from the $PDK1^{fl/fl}$ CRE^{-} and $PDK1^{fl/fl}$ CRE^{+} mice, that are homozygous for the conditional, leaky allele, in comparison to the $PDK1^{+/fl}$ CRE^{-} and $PDK1^{+/fl}$ CRE^{+} controls, which retain a wild type copy of the PDK1 gene (Fig. 1C).

The resultant $PDK1^{fl/fl}$ CRE^{+} mutant mice as well as the $PDK1^{fl/fl}$ CRE^{-} control mice, which also express high levels of the PDK1 L155E mutant protein in non-neuronal tissues (Fig. 1C), were viable, fertile, and displayed a 25% reduction in body weight compared to $PDK1^{+/fl}$ CRE^{-} mice, which retain a wild type copy for the PDK1 gene (Fig. 2B). Stereological analysis demonstrated that both the brain and the head volumes were proportionally reduced by 20% in the $PDK1^{fl/fl}$ CRE^{-} and $PDK1^{fl/fl}$ CRE^{+} E15,5 embryos when compared to the $PDK1^{+/fl}$ CRE^{-} controls (Fig. 2A, C). While the $PDK1^{fl/fl}$ CRE^{-} mice exhibited a 25% reduction in both the volume and the mass of the brain when compared to the $PDK1^{+/fl}$ CRE^{-} controls which is proportional to the reduction in the body weight, the $PDK1^{fl/fl}$ CRE^{+} adult mutant mice exhibited microcephaly, with brains showing a reduction

of about 50% in volume and mass than those from the PDK1$^{+/fl}$ CRE^{-} controls (Fig 2D). Determination of the volume of the neuronal soma and the number of neuronal cells purified at E15,5 from the embryonic cortex suggested that the small brain size of the PDK1$^{fl/fl}$ CRE^{-} and PDK1$^{fl/fl}$ CRE^{+} mice might be mostly due to a reduction in the size of the cells rather than to reduced number of cells (Fig. 2E, F).

S6K, RSK, SGK and PKC are not activated in the PDK1$^{fl/fl}$ CRE^{+} brain.

To define the importance of the PDK1 substrate-docking site in the ability of PDK1 to activate its different cellular targets, primary cultures of cortical neurons derived from littermate PDK1$^{+/fl}$ CRE^{-}, PDK1$^{fl/fl}$ CRE^{-} and PDK1$^{fl/fl}$ CRE^{+} embryos were stimulated with BDNF for 15 minutes. As a control of the stimulation, the activation of the BDNF receptor TrkB was monitored by measuring its phosphorylation at the activation loop residues Tyr706/707, which was very robust in all the three genotypes analyzed (Fig 3A). By contrast, phosphorylation of TrkB was not detectable in whole brain tissue lysates at E15,5, despite the high levels of expression of the receptor (Fig 3B).

BDNF induced a clear activation of Akt to the same extent in all the three genotypes analyzed, as judged by the level of phosphorylation of the two activating residues, Thr308 and Ser473. This was corroborated by measuring the phosphorylation levels of the Akt substrate PRAS40 at Thr246, which was not affected by the PDK1 L155E mutation (Fig 3A). To further validate this data in a more physiological context, the levels of phosphorylation and activation of Akt were also measured in whole protein extracts derived from the E15,5 developing brain, which were similar in all the three different genotypes analyzed (Fig. 3B).

By contrast, phosphorylation of S6K at the T-loop Thr229 site by PDK1 was markedly reduced in the PDK1$^{fl/fl}$ CRE^{-} cell and tissue samples when compared with the PDK1$^{+/fl}$

CRE$^-$ controls, and almost abolished in the PDK1$^{fl/fl}$ CRE$^+$ samples. As a consequence, S6K activation, as monitored by the phosphorylation of the S6 ribosomal protein at Ser235, was similarly affected (Fig. 3).

BDNF also induced a robust autophosphorylation of the Ser380 hydrophobic motif site of RSK and the consequent recognition and phosphorylation of the Ser227 T-loop site by PDK1 (34) in the PDK1$^{+/fl}$ CRE$^-$ control cells**.** By contrast, phosphorylation of RSK at Ser227 by PDK1 was gradually reduced in the PDK1$^{fl/fl}$ CRE$^-$ and PDK1$^{fl/fl}$ CRE$^+$ cells and tissues (Fig. 3)**.**

Activation of SGK1 requires the phosphorylation of the hydrophobic motif at Ser422 by mTORC2, which primes the binding of PDK1 (35). As expected, BDNF-induced phosphorylation of SGK1 at the Thr256 PDK1 site within the T-loop was reduced in the PDK1$^{fl/fl}$ CRE$^-$ cortical cultures when compared with the PDK1$^{+/fl}$ CRE$^-$ controls, and further decreased in the PDK1$^{fl/fl}$ CRE$^+$ samples and tissues (Fig. 3).

PDK1 also controls the stability of PKC isoforms through the phosphorylation of their T-loop sites (36). We found both the levels of phosphorylation as well as the levels of expression of PKCα reduced in the PDK1$^{fl/fl}$ CRE$^+$ cells and tissues (Fig. 3) compared to the PDK1$^{fl/fl}$ CRE$^-$ and PDK1$^{+/fl}$ CRE$^-$ samples.

Binding of the PDK1 PIF-pocket to the substrate docking site is not essential to support neuronal survival.

The neuronal-specific PDK1 PIF-pocket mutation most likely compromised growth responses during brain development, leading to microcephaly in the PDK1$^{fl/fl}$ CRE$^+$ mutant adult mice. It is well known than the PI3K/PDK1/Akt signaling pathway plays critical roles in mediating the responses to survival signals that antagonize the intrinsic programmed cell death in the developing nervous system (6,37). We recently showed how decreasing the

efficiency of PKB/Akt activation by expressing the mutant form of PDK1 K465E incapable of phosphoinositide binding had no consequences on neuronal survival (22). From that it was postulated that either the reduced levels of Akt activity attained in the $PDK1^{K465E/K465E}$ mice were sufficient to preserve normal neuronal viability, or that other PDK1-activated kinases different from Akt were responsible for transducing the survival program elicited by extracellular signals. To address this question, we took advantage of the PDK1 L155E neuronal-specific knock-in mice. Neuronal programmed cell death can be accurately recapitulated in vitro in primary cultures of embryonic cortical neurons, which survive in the presence of particular neurotrophins such as BDNF and die through apoptosis upon trophic factor withdrawal. Trophic factor deprivation induced the death of about half of the cells, as denoted by a fifty per cent decrease in the MTT reduction values (Fig 4A) and a five-fold increase in the number of apoptotic cells (Fig 4B-C) in all the four genotypes analyzed. BDNF completely recovered the cell viability values (Fig 4A) while decreasing by two to three-folds the number of cells exhibiting apoptosis (Fig 4B-C) to the same extent in all the four genotypes analyzed. From this it was concluded that the PDK1 PIF-pocket dependent AGC kinases were neither essential for the neuroprotective actions of BDNF, at least in cortical neurons.

We next measured proliferation as well as cell death parameters on primary cultures of cortical neurons during the first four days in vitro by using the Ki67 proliferation marker and the cleaved/active caspase-3 apoptotic marker. At day in vitro 0 (DIV0), the $PDK1^{+/fl}$ CRE^{-} control cultures reached highest proliferation rates above 20%, which were significantly reduced in both the $PDK1^{fl/fl}$ CRE^{-} and $PDK1^{fl/fl}$ CRE^{+} cultured cortical neurons (Fig 5A,B). This proliferating activity, most likely corresponding to the neurogenesis peak of those progenitors that will populate later the upper cortical layers,

vastly ceased as the cells progressed to DIV4, which was accompanied by a moderate increase in the apoptotic index to similar levels in all three genotypes analyzed (Fig 5A,C). Accordingly, coronal brain sections from E15,5 embryos stained with the newly born neurons marker Doublecortin revealed a clear reduction of the neuronal progenitor cells in the $PDK1^{fl/fl}$ CRE^{-} and $PDK1^{fl/fl}$ CRE^{+} embryos compared to the $PDK1^{+/fl}$ CRE^{-} controls (Fig 5D,E). By contrast, no evidence of apoptosis was observed in any of the three genotypes analyzed, as judged by the nearly absence of active caspase-3 staining (Fig 5D,F). Since soma size analysis of hippocampal neurons in culture revealed a genotype dependent decrease in the diameter of the cellular soma (Fig. 6D), altogether our data demonstrates a combined reduction in progenitor proliferation and cell growth responses.

PDK1 promotes neuronal polarization and axonal outgrowth through the PIF-pocket dependent substrates.

The PI 3-kinase signaling pathway controls several aspects of neuronal morphogenesis including neuronal polarization, axonal outgrowth and dendrite arborization (38). In the $PDK1^{K465E/K465E}$ mice, the Akt/mTORC1 axis was instructive for PI 3-kinase mediated neuronal polarization and axon outgrowth (22). Since S6K is a major effector of mTORC1 in controlling the translation of proteins that are relevant for neuronal differentiation, we reasoned that the PDK1 L155E mice model, with normal levels of Akt activity but in which S6K cannot be activated by PDK1, could be instrumental in defining the contribution of S6K to neuronal differentiation. To that end, we analyzed cell polarization and measured the axon length during the differentiation of hippocampal primary neurons in culture. In the $PDK1^{+/fl}$ CRE^{-} control cultures, most of the neurons exhibited a differentiated axon by DIV3, as denoted by the expression of the axonal specific microtubule-associated protein Tau-1. By contrast, neuronal polarization was severely impaired in both the $PDK1^{fl/fl}$ CRE^{-}

and PDK1$^{fl/fl}$ CRE^{+} mutant hippocampal cultures, in which only half of the neurons showed axons by DIV3 and 4 (Fig 6A,B). The complexity of the neuritic processes, as inferred from the number of neurites per cell (Fig 6C), as well as their length and the amount of ramifications (Fig 6E), was similar in PDK1$^{+/fl}$ CRE^{-}, PDK1$^{fl/fl}$ CRE^{-} and PDK1$^{fl/fl}$ CRE^{+} mice hippocampal neurons at all the time points analyzed. By contrast, the average length of the axon was reduced by thirty per cent in the PDK1$^{fl/fl}$ CRE^{-} neurons and as much as forty per cent in the PDK1$^{fl/fl}$ CRE^{+} neurons when compared to the PDK1$^{+/fl}$ CRE^{-} control cells, both at DIV3 and 4 (Fig 6E).

Reduced connectivity and abnormal cortical layering in the mutant mice adult brain. We next explored how the deficient differentiation abilities of the PDK1$^{fl/fl}$ CRE^{-} and PDK1$^{fl/fl}$ CRE^{+} embryonic neurons detected ex vivo had physiological consequences in the adult brain. Immunostaining of brain sections with antibodies to microtubule-associated proteins that are selectively localized in either axons (SMI312) or dendrites (MAP2) revealed a clear decrease in the density of axonal fibers in various regions of the PDK1$^{fl/fl}$ CRE^{-} and PDK1$^{fl/fl}$ CRE^{+} cortex (Fig 7A) and hippocampus (Fig 7B), in a genotype dose-dependent manner.

The PI 3-kinase signaling pathway also controls the radial migration of new-born cortical neurons during cortex development, resulting in an ordered arrangement of neurons into six different cortical layers. It has been proposed that Akt, but not mTORC1, controls cortical development downstream of PI 3-kinase activation (39). Since the neuronal differentiation program is integrated with the program of neuronal migration, we aimed to determine whether the PI 3-kinase/PDK1 effectors that are independent of Akt activation were also important for cortical development. We observed that in the PDK1$^{fl/fl}$ CRE^{-} adult brain, neurons in layer IV of the somatosensory cortex were packed together (Fig 8B) and further

compacted in the PDK1$^{fl/fl}$ CRE^{+} mice (Fig 8C) when compared to the PDK1$^{+/fl}$ CRE^{-} controls (Fig 8A), as revealed by immunohistochemical analysis with the NeuN neuronal marker.

Cortical layer IV is mainly composed of pyramidal neurons and gabaergic interneurons. For that reason, we employed antibodies against CUX1, a transcription factor which is expressed in glutamatergic cortical neurons from upper layers II to IV of the somatosensory cortex, and GAD67, the decarboxylase which catalyze the conversion of glutamate to the GABA inhibitory neurotransmitter in the gabaergic interneurons. While CUX1 staining confirmed that the neuronal packing arises from an increase in the glutamatergic neurons cell density with normal number of cells (Fig 9A-D), a clear decrease in the GAD67 expression in the somatosensory cortex (Fig 9A,E) and cingulated cortex (Fig 9F) was observed, arising from the increase in the PDK1 L155E mutant protein levels across the different genotypes analyzed. Moreover, the parvalbumin-positive interneurons were mostly excluded from layer IV in the PDK1$^{fl/fl}$ CRE^{+} cortex samples when compared with its distribution in the PDK1$^{fl/fl}$ CRE^{-} and PDK1$^{+/fl}$ CRE^{-} cortex (Fig 9B).

Neuropsychiatric-like behaviors in the brain-specific PDK1 L155E mutant mice.

A three-stage protocol for behavioral and functional comprehensive phenotype assessment of mutant mice (28,29) evaluated the physical condition, sensorimotor functions, behavioral and psychological profiles (spontaneous behavior, locomotor and exploratory activities, anxious-like behaviors, motivation) as well as cognition (learning and memory, attention, executive functions). Somatic growth, as measured by body weight, was reduced with lower food intake (Fig 10A). Sensorimotor functions were severely reduced by two-fold, even in an easy task as the wood rod test (Fig 10B). A deficiency in a highly preserved daily life ethological activity such as nesting behavior evidenced impairment of executive

functions (Fig 10C). The mutant mice showed apparent undisturbed behavior in the homecage, with normal socialization and sleeping in groups but absence of barbering. Disrupted behavior aroused when handled, with high incidence of hyper-reactivity shown as rejection to be handled (5/6), vocalizations (3/6), bizarre behaviors (4/6) (Fig 10D, stereotyped stretching), refusal to perform the tests such as the hanger test (6/6) and diminished motivation to swim in the water maze (Fig 10G, flotation). Neophobia in the corner test suggested a flight-behavior, which in a more anxiogenic environment such as the open-field test (Fig 10E), turned into freezing behavior. An overall reduced total vertical exploratory activity was observed, while the thigmotaxis ratio (locomotion in the periphery vs center) was maintained in the mutants. These results were confirmed in the 84h continuous circadian activity recordings in a cage equipped with a wheel (Fig 10H). In that setting, the time course from the first (novelty) to the fourth (habituation) night was strikingly reduced in the mutant mice, mostly within the first two nocturnal activity periods. In the marble burying test, the mutants exhibited a higher number of marbles changed of position, in detriment of the number of buried pieces (Fig 10F). With respect to their cognitive abilities, both groups solved equally the first experience in the water maze. However, a poorest acquisition curve was seen in the mutant group, resulting in a worse cognitive capacity at the end of the perceptual visual learning paradigm which involves attention and motivation (Fig 10G, CUE1-4). Similarly, on the following days, mutant mice showed cognitive deficits in their spatial learning and memory abilities in the place learning task. They performed similarly in the first trial of each day (long-term memory) but did not progress successfully in the trial-by-trial test (short-term and working memory), again with a worse learning curve and ratios, as compared to their age matched wild-type group. A higher incidence of periods of immobility (flotation), as a non-searching behavior

494 indicative of changes in motivation in the mutants, was also shown all through the test (Fig
495 10G).

Discussion

In the present study we characterized the Akt-independent roles that the PDK1 signaling pathway plays during brain development. Disrupting the interaction of PDK1 with its substrates in the $PDK1^{L155E/L155E}$ full knock-in mice resulted in an embryonic lethal phenotype, with embryos dying at E12 exhibiting severe retardation and a major reduction in the forebrain size, thereby highlighting the essential roles that the Akt independent branch of the PDK1 signaling network played during embryonic development (23,40). To circumvent this lethal period, we targeted the expression of the PDK1 L155E mutant protein to neuronal tissues by conditional knock-in methodologies. The $PDK1^{fl/fl}$ CRE^{+} genotype was observed at birth at a three-fold reduced mendelian frequency. By contrast, the $PDK1^{fl/fl}$ CRE^{-} controls were born at the expected frequency, thus indicating that low levels of PDK1 wild type protein were sufficient for the $PDK1^{fl/fl}$ CRE^{-} mice to complete embryonic development, and that the further and specific ablation of the wild type PDK1 sequence in the nervous system was responsible for the lethality of the $PDK1^{fl/fl}$ CRE^{+} mutant embryos. The hypomorphic nature of the PDK1 L155E conditional knock-in allele, which can drive the expression of as much as sixty-seventy per cent of PDK1 L155E mutant protein without compromising the viability of these mice, makes the $PDK1^{fl/fl}$ conditional knock-in mice an excellent genetic tool to study the function of PDK1 beyond Akt in a more physiological context. At the same time, these mice could represent the appropriate experimental model to validate the effects of new allosteric modulators targeting the PDK1 PIF-pocket, which are nowadays being developed and hold an enormous therapeutic potential (41).

518 Activation of S6K, RSK, SGK and PKC, but not Akt, was selectively decreased in the
519 PDK1$^{fl/fl}$ CRE^{-} mouse cortical neurons, when compared to the PDK1$^{+/fl}$ CRE^{-} controls, and
520 further abolished in the PDK1$^{fl/fl}$ CRE^{+} neuronal cells and tissues. We and others recently
521 described how in the absence of PtdIns(3,4,5)P_3 binding, PDK1 can still activate Akt by
522 binding to the phosphorylated Akt hydrophobic motif (42,43). In agreement with that, in
523 the PDK1$^{K465E/K465E}$ knock-in mice expressing a mutant form of PDK1 incapable of
524 phosphoinositide binding, activation of Akt was selectively affected, but not fully abolished
525 (22). By contrast, in the PDK1$^{fl/fl}$ CRE^{+} neurons and tissues, Akt was normally activated,
526 thereby demonstrating that in physiological conditions, Akt activation by PDK1 rely mostly
527 on the phosphoinositide-mediated co-localization of both kinases at PtdIns(3,4,5)P_3-rich
528 cellular membranes rather than on the docking site interaction.
529 The reduced phosphorylation of S6K and RSK at their activation loops by PDK1 arises
530 from the inability of the PDK1 L155E mutated PIF-pocket to interact with the phospho-
531 hydrophobic motif docking site in S6K and RSK. Unexpectedly, the level of
532 phosphorylation of S6K at the Thr389 and RSK at the Ser380 hydrophobic motif sites was
533 also decreased to the same extent than that of the activation loops. The AGC kinases
534 possess and hydrophobic groove in the small lobe of their kinase domains similar to the
535 PDK1 PIF-pocket. This hydrophobic pocket establishes intramolecular interactions with the
536 phosphorylated hydrophobic motif that are fundamental for the transition of the enzyme to
537 the active conformation (44). In the absence of activation loop phosphorylation, the active,
538 closed conformation is not favored, which may allow the exposure of the hydrophobic
539 motif phosphorylation site to the action of phosphatases (23).
540 PDK1 plays a major role in the processing and maturation of several PKC isoforms. Newly
541 synthesized PKC polypeptides are first phosphorylated at their hydrophobic motifs

allowing PDK1 to interact and phosphorylate the T-loops. These first phosphorylation events do not depend on apical agonist-stimulation, and stabilize the enzyme in a catalytically inactive conformation but at the same time competent to respond to the diacylglycerol and calcium second messengers (45,46). In agreement with that notion, both the levels of phosphorylation as well as the levels of expression of PKCα were reduced in the $PDK1^{fl/fl}$ CRE^{+} embryonic brain samples as well as cortical cell extracts, but not in the $PDK1^{fl/fl}$ CRE^{-} samples when compared to the $PDK1^{+/fl}$ CRE^{-} controls (Fig. 3), thereby indicating that the reduced levels of expression of the wild type PDK1 protein in the $PDK1^{fl/fl}$ CRE^{-} mice were sufficient to regulate phosphorylation and stability of PKC isoforms, which was unchanged upon BDNF stimulation of cortical neurons (Fig 3A). One salient finding derived from these studies is that disrupting the interaction of PDK1 with their substrates in the $PDK1^{fl/fl}$ CRE^{+} mutant mice has not consequences regarding neuronal survival. This is consistent with the fact that the PKB/Akt kinase, which is the only PDK1 substrate that is not affected by the PDK1 L155E mutation, is thought to be the critical downstream effector of this pathway in promoting survival by antagonizing the programmed cell death (47). However, in the $PDK1^{K465E/K465E}$ knock-in mice, reduced activation of Akt isoforms was also sufficient to dictate neuronal survival (22). We recently demonstrated how the inhibition of mTORC2, the Akt and SGK hydrophobic motif kinase, modestly compromised the viability of the PDK1 wild type neurons at doses that did not affect Akt activation, and that was further aggravated in the $PDK1^{K465E/K465E}$ mutant neurons (43). Altogether, these results point out to a synergistic role of both Akt and SGK in controlling neuronal survival by coordinately regulating the phosphorylation of some substrates that are relevant to the control of apoptosis. By contrast, both cell proliferation and cell growth were reduced in the $PDK1^{fl/fl}$ CRE^{+} mutant mice, which might arise from

566 the inability of PDK1 to activate S6K despite unaffected PI3K/Akt/mTORC1 signaling.
567 These results situate S6K as the most critical downstream effector of this signaling pathway
568 in instructing cell and organism growth.
569 The observation that both the neuronal polarization and axonal elongation responses of
570 hippocampal neurons from the $PDK1^{fl/fl}$ CRE^{-} and $PDK1^{fl/fl}$ CRE^{+} mice were inhibited by
571 the PDK1 PIF-pocket mutation is particularly relevant, since the establishment of the axon-
572 dendrite axis is an essential morphogenetic mechanism for the appropriate assembly of
573 neurons onto functional neuronal circuits. This process is triggered by different
574 extracellular signals acting through a number of intracellular signaling pathways. Among
575 them, the interplay between the PI3K/Akt signaling pathway (48), the Par3-Par6-aPKC
576 complexes (4) and the LKB1/BRSK axis (49,50) is fundamental in controlling axon
577 specification and growth. In agreement with that, in the $PDK1^{K465E/K465E}$ mice, the
578 PI3K/Akt/mTORC1-dependent regulation of the BRSK protein levels represents an
579 integration point for both the PI3K and LKB1 signaling pathways in axonal morphogenesis
580 (22). In these mice, the hypomorphic reduction of the Akt signaling towards the
581 PRAS40/TSC2/mTORC1/S6K axis caused mild phenotypes that could be mimicked ex
582 vivo with the Akti-1/2 inhibitory compound, which reduced Akt activity by inhibiting the
583 Akt1 and Akt2, but not the Akt3 isoform, and aggravated by using the mTORC1 inhibitor
584 rapamycin. Interestingly, in the $PDK1^{fl/fl}$ CRE^{-} and $PDK1^{fl/fl}$ CRE^{+} mice, in which the
585 PI3K/Akt/mTORC1 axis is normally activated, the defects in both the polarity and the
586 axonal elongation processes were more severe that those reported in the $PDK1^{K465E/K465E}$
587 mice, which phenocopied the severe differentiation defects previously observed with the
588 mTORC1 inhibitor (22). Altogether, these observations place a PIF-pocket dependent
589 kinase, namely S6K, as a key effector of the PI3K/Akt/mTORC1 axis in controlling the

590 synthesis of proteins that are relevant for neuronal morphogenesis. Moreover, while in the
591 PDK1$^{K465E/K465E}$ mice the transient alterations in the timing of the differentiation program
592 did not translate onto gross abnormalities in the patterning of the adult brain (22), the
593 genetic ablation of S6K activation with intact Akt signaling in the PDK1$^{fl/fl}$ CRE^{+} adult
594 mice caused microcephaly with profound structural and molecular brain alterations, thereby
595 ruling out the implication of other Akt or mTORC1 substrates different from S6K on these
596 phenotypes.
597 Further experiments must be undertaken in the future to elucidate the connection between
598 the impaired PDK1 PIF-pocket-dependent signaling in mutant mice and the altered
599 population of interneurons denoted by the GAD67 and parvoalbumin markers defects. In
600 this regard, defects in the translation machinery in neurons caused by elongator subunit
601 Elp3 deletion have been recently related to impaired neuronal differentiation and
602 imbalanced neurogenesis, leading to microcephaly resulting from the premature migration
603 of neurons (51,52). In an analog form, the S6K PIF-pocket dependent kinase is
604 indispensable for the pre-initiation complex (PIC) formation and protein translation (53,54).
605 Abrogation of S6K activation in the PDK1 L155E mutant mice could have impaired the
606 normal protein translation in neurons leading to imbalanced neurogenesis, thereby
607 generating a potential molecular connection between the PIF-pocket mutation and the
608 described brain defects associated to microcephaly. Moreover, the deficient polarization
609 and axonal outgrowth of the PDK1 L155E mutant neurons might have caused altered
610 migration patterns during cortex lamination, contributing to the decreased density of axonal
611 fibers in the cortex and hippocampus, increased density of glutamatergic neurons with
612 normal number of cells in cortical layers II-IV, decreased GAD67 expression levels, and
613 miss-localized parvalbumin-positive interneurons, which were mostly excluded from layer

614 IV. Intriguingly, these alterations are commonly observed in human mental diseases such as
615 schizophrenia. These included reduced axonal density in the cortex and the hippocampus
616 (55), elevated neuronal density in cortical layer IV (56), GAD67 deficits in the upper
617 cortical layers, especially in the cingulated cortex (57), and abnormal localization of the
618 parvalbumin positive interneurons (58). The current hypotheses on the etiology of
619 schizophrenia state that this molecular and structural scenario is thought to result in
620 deregulated GABAergic interneuron-mediated inhibition of glutamatergic neurons,
621 resulting in an over-activation of the neuronal circuits and contributing in this manner to the
622 characteristic symptoms of this disease.
623 In the $PDK1^{fl/fl}$ CRE^{+} mice, the behavioral disturbances included a wide array of
624 impairments, ranging from sensorimotor and basic species executive functions, to both
625 cognitive and non-cognitive behavioral alterations. The different tests assessed convey to
626 point out to relevant and persistent bizarre behaviors, severe reduction of exploratory
627 activity, increased freezing, diminished motivation and impaired short-term working
628 memory. Much future work need to be performed to define whether the presence of both
629 exacerbated disruptive behavior suggesting an hypersensitivity to stressful situations, but
630 reduced activity and diminished motivation would have face validity for negative
631 symptoms that characterize the clinical features of the schizophrenia spectrum (59).
632 Moreover, cognitive impairment with affection of learning and memory but also attention
633 and executive functions, would be also compatible with cognitive clinical symptoms of
634 schizophrenia.
635 Human schizophrenia might arise from an inherited genetic predisposition causing brain
636 developmental alterations combined with environmental factors that can influence brain
637 maturation during the childhood. A number of genes that have been associated to familiar

638 forms of schizophrenia converge onto the same signaling pathway. These include the
639 neuregulin-1 (NRG1) growth factor coding-gene (60,61), the dystrobrevin-binding protein
640 1 (DTNBP1) gene (12) the DISC1 scaffolding protein coding gene (13), as well as the Akt1
641 gene (11), which altogether participate in the modulation of the Akt signaling outputs. To
642 our knowledge, this is the first report evidencing the involvement of PDK1 downstream
643 effectors different from Akt in mice neuropsychiatric-like disorders, with potential face and
644 construct validity for negative and cognitive symptoms of schizophrenia. Our results point
645 out to a prominent function for PIF-pocket dependent kinases as major effectors of this
646 signaling hub downstream of Akt in the etiopathogenesis of schizophrenia that might
647 provide construct validity to the PDK1 L155E mutants.
648

ACKNOWLEDGMENTS

We thank Dario Alessi (MRC Protein Phosphorylation Unit, Dundee, UK) for providing the mice and some of the antibodies; Cristina Gutierrez, Mar Castillo and Núria Barba (Cell Culture, Histology and Microscopy Services of the Institut de Neurociències) for technical assistance; Jessica Pairada and Núria Moix (Estabulari de Rosegadors of the Universitat de Lleida) for animal care; time allocated in the joint nuclear magnetic resonance facility of the Universitat Autònoma de Barcelona and Centro de Investigación Biomédica en Red-Bioingeniería, Biomateriales y Nanomedicina (CIBER-BBN) (Cerdanyola del Vallès, Spain). The authors want to express their gratitude to Alfredo Miñano and Montse Solé for helpful discussion and to Arnaldo Parra, Lilian Enríquez and Carles Saura for their expert advice on mice brain development.

Ll.C.B., J.R.B., J.M.L. and E.C. designed the experiments, analyzed the data and wrote the manuscript. Ll.C.B performed most of the biochemical, cell biology, survival, differentiation and brain anatomopathological experiments. S.P.G. conducted the stereological analysis as well as the proliferation and apoptosis studies. S.Y. and S.P.G. carried out the signaling analysis. C.N. helped with the differentiation studies. S.L.P. assisted with the MRI analysis. L.G.L. carried out the behavioral characterization. J.R.B. managed and genotyped the mice colonies.

FUNDING INFORMATION.

JRB is a Serra Húnter Fellow of the Catalan Government. SY was supported by a Fellowship of the Chinese Scholarship Council (CSC). The funders had no role in study design, data collection and interpretation, or the decision to submit the work for publication.

We have no relevant conflicts of interest to disclose.

673 REFERENCES
674

675 1. **Vanhaesebroeck B, Stephens L, Hawkins P.** 2012. PI3K signalling: the path to
676 discovery and understanding. Nat. Rev. Mol. Cell Biol. **13**:195-203.

677 2. **Engelman JA, Luo J, Cantley LC.** 2006. The evolution of phosphatidylinositol 3-
678 kinases as regulators of growth and metabolism. Nat. Rev. Genet. **7**:606-619.

679 3. **Choi YJ, Di NA, Kramvis I, Meikle L, Kwiatkowski DJ, Sahin M, He X.** 2008.
680 Tuberous sclerosis complex proteins control axon formation. Genes Dev. **22**:2485-
681 2495.

682 4. **Shi SH, Jan LY, Jan YN.** 2003. Hippocampal neuronal polarity specified by
683 spatially localized mPar3/mPar6 and PI 3-kinase activity. Cell **112**:63-75.

684 5. **Jiang H, Guo W, Liang X, Rao Y.** 2005. Both the establishment and the
685 maintenance of neuronal polarity require active mechanisms: critical roles of GSK-
686 3beta and its upstream regulators. Cell **120**:123-135.

687 6. **Brunet A, Datta SR, Greenberg ME.** 2001. Transcription-dependent and -
688 independent control of neuronal survival by the PI3K-Akt signaling pathway. Curr.
689 Opin. Neurobiol. **11**:297-305.

690 7. **Chalhoub N, Zhu G, Zhu X, Baker SJ.** 2009. Cell type specificity of PI3K
691 signaling in Pdk1- and Pten-deficient brains. Genes Dev. **23**:1619-1624.

692 8. **Eickholt BJ, Ahmed AI, Davies M, Papakonstanti EA, Pearce W, Starkey ML,**
693 **Bilancio A, Need AC, Smith AJ, Hall SM, Hamers FP, Giese KP, Bradbury EJ,**
694 **Vanhaesebroeck B.** 2007. Control of axonal growth and regeneration of sensory
695 neurons by the p110delta PI 3-kinase. PLoS. One. **2**:e869.

696 9. **Kwon CH, Luikart BW, Powell CM, Zhou J, Matheny SA, Zhang W, Li Y,**
697 **Baker SJ, Parada LF.** 2006. Pten regulates neuronal arborization and social
698 interaction in mice. Neuron **50**:377-388.

699 10. **Tohda C, Nakanishi R, Kadowaki M.** 2009. Hyperactivity, memory deficit and
700 anxiety-related behaviors in mice lacking the p85alpha subunit of phosphoinositide-3
701 kinase. Brain Dev. **31**:69-74.

702 11. **Emamian ES, Hall D, Birnbaum MJ, Karayiorgou M, Gogos JA.** 2004.
703 Convergent evidence for impaired AKT1-GSK3beta signaling in schizophrenia. Nat.
704 Genet. **36**:131-137.

705 12. **Guo AY, Sun J, Riley BP, Thiselton DL, Kendler KS, Zhao Z.** 2009. The
706 dystrobrevin-binding protein 1 gene: features and networks. Mol. Psychiatry **14**:18-29.

707 13. **Chubb JE, Bradshaw NJ, Soares DC, Porteous DJ, Millar JK.** 2008. The DISC
708 locus in psychiatric illness. Mol. Psychiatry **13**:36-64.

14. **Butler MG, Dasouki MJ, Zhou XP, Talebizadeh Z, Brown M, Takahashi TN, Miles JH, Wang CH, Stratton R, Pilarski R, Eng C.** 2005. Subset of individuals with autism spectrum disorders and extreme macrocephaly associated with germline PTEN tumour suppressor gene mutations. J. Med. Genet. **42**:318-321.

15. **Zhou J, Parada LF.** 2012. PTEN signaling in autism spectrum disorders. Curr. Opin. Neurobiol. **22**:873-879.

16. **Alessi DR, James SR, Downes CP, Holmes AB, Gaffney PR, Reese CB, Cohen P.** 1997. Characterization of a 3-phosphoinositide-dependent protein kinase which phosphorylates and activates protein kinase Balpha. Curr. Biol. **7**:261-269.

17. **Bayascas JR.** 2010. PDK1: the major transducer of PI 3-kinase actions. Curr. Top. Microbiol. Immunol. **346**:9-29.

18. **Pearce LR, Komander D, Alessi DR.** 2010. The nuts and bolts of AGC protein kinases. Nat. Rev. Mol. Cell Biol. **11**:9-22.

19. **Biondi RM, Komander D, Thomas CC, Lizcano JM, Deak M, Alessi DR, Van Aalten DM.** 2002. High resolution crystal structure of the human PDK1 catalytic domain defines the regulatory phosphopeptide docking site. EMBO J. **21**:4219-4228.

20. **Frodin M, Antal TL, Dummler BA, Jensen CJ, Deak M, Gammeltoft S, Biondi RM.** 2002. A phosphoserine/threonine-binding pocket in AGC kinases and PDK1 mediates activation by hydrophobic motif phosphorylation. EMBO J. **21**:5396-5407.

21. **Bayascas JR.** 2008. Dissecting the role of the 3-phosphoinositide-dependent protein kinase-1 (PDK1) signalling pathways. Cell Cycle **7**:2978-2982.

22. **Zurashvili T, Cordon-Barris L, Ruiz-Babot G, Zhou X, Lizcano JM, Gomez N, Gimenez-Llort L, Bayascas JR.** 2013. Interaction of PDK1 with Phosphoinositides Is Essential for Neuronal Differentiation but Dispensable for Neuronal Survival. Mol. Cell Biol. **33**:1027-1040.

23. **Collins BJ, Deak M, Arthur JS, Armit LJ, Alessi DR.** 2003. In vivo role of the PIF-binding docking site of PDK1 defined by knock-in mutation. EMBO J. **22**:4202-4211.

24. **Tronche F, Kellendonk C, Kretz O, Gass P, Anlag K, Orban PC, Bock R, Klein R, Schutz G.** 1999. Disruption of the glucocorticoid receptor gene in the nervous system results in reduced anxiety. Nat. Genet. **23**:99-103.

25. **Bayascas JR, Sakamoto K, Armit L, Arthur JS, Alessi DR.** 2006. Evaluation of approaches to generation of tissue-specific knock-in mice. J. Biol. Chem. **281**:28772-28781.

26. **Kilkenny C, Browne WJ, Cuthill IC, Emerson M, Altman DG.** 2010. Improving bioscience research reporting: The ARRIVE guidelines for reporting animal research. J. Pharmacol. Pharmacother. **1**:94-99.

27. **Gundersen HJ, Jensen EB.** 1987. The efficiency of systematic sampling in stereology and its prediction. J. Microsc. **147**:229-263.

28. **Gimenez-Llort L, Fernandez-Teruel A, Escorihuela RM, Fredholm BB, Tobena A, Pekny M, Johansson B.** 2002. Mice lacking the adenosine A1 receptor are anxious and aggressive, but are normal learners with reduced muscle strength and survival rate. Eur. J. Neurosci. **16**:547-550.

29. **Rogers DC, Fisher EM, Brown SD, Peters J, Hunter AJ, Martin JE.** 1997. Behavioral and functional analysis of mouse phenotype: SHIRPA, a proposed protocol for comprehensive phenotype assessment. Mamm. Genome **8**:711-713.

30. **Torres-Lista V, Gimenez-Llort L.** 2013. Impairment of nesting behaviour in 3xTg-AD mice. Behav. Brain Res. **247**:153-157.

31. **Garcia-Mesa Y, Lopez-Ramos JC, Gimenez-Llort L, Revilla S, Guerra R, Gruart A, LaFerla FM, Cristofol R, gado-Garcia JM, Sanfeliu C.** 2011. Physical exercise protects against Alzheimer's disease in 3xTg-AD mice. J. Alzheimers. Dis. **24**:421-454.

32. **Balendran A, Casamayor A, Deak M, Paterson A, Gaffney P, Currie R, Downes CP, Alessi DR.** 1999. PDK1 acquires PDK2 activity in the presence of a synthetic peptide derived from the carboxyl terminus of PRK2. Curr. Biol. **9**:393-404.

33. **Biondi RM, Cheung PC, Casamayor A, Deak M, Currie RA, Alessi DR.** 2000. Identification of a pocket in the PDK1 kinase domain that interacts with PIF and the C-terminal residues of PKA. EMBO J. **19**:979-988.

34. **Anjum R, Blenis J.** 2008. The RSK family of kinases: emerging roles in cellular signalling. Nat. Rev. Mol. Cell Biol. **9**:747-758.

35. **Garcia-Martinez JM, Alessi DR.** 2008. mTOR complex 2 (mTORC2) controls hydrophobic motif phosphorylation and activation of serum- and glucocorticoid-induced protein kinase 1 (SGK1). Biochem. J. **416**:375-385.

36. **Balendran A, Hare GR, Kieloch A, Williams MR, Alessi DR.** 2000. Further evidence that 3-phosphoinositide-dependent protein kinase-1 (PDK1) is required for the stability and phosphorylation of protein kinase C (PKC) isoforms. FEBS Lett. **484**:217-223.

37. **Kharebava G, Makonchuk D, Kalita KB, Zheng JJ, Hetman M.** 2008. Requirement of 3-phosphoinositide-dependent protein kinase-1 for BDNF-mediated neuronal survival. J. Neurosci. **28**:11409-11420.

38. **Waite K, Eickholt BJ.** 2010. The neurodevelopmental implications of PI3K signaling. Curr. Top. Microbiol. Immunol. **346**:245-265.

39. **Jossin Y, Goffinet AM.** 2007. Reelin signals through phosphatidylinositol 3-kinase and Akt to control cortical development and through mTor to regulate dendritic growth. Mol. Cell Biol. **27**:7113-7124.

40. **McManus EJ, Collins BJ, Ashby PR, Prescott AR, Murray-Tait V, Armit LJ, Arthur JS, Alessi DR.** 2004. The in vivo role of PtdIns(3,4,5)P3 binding to PDK1 PH domain defined by knockin mutation. EMBO J. **23**:2071-2082.

41. **Arencibia JM, Pastor-Flores D, Bauer AF, Schulze JO, Biondi RM.** 2013. AGC protein kinases: From structural mechanism of regulation to allosteric drug development for the treatment of human diseases. Biochim. Biophys. Acta **1834**:1302-1321.

42. **Najafov A, Shpiro N, Alessi DR.** 2012. Akt is efficiently activated by PIF-pocket- and PtdIns(3,4,5)P3-dependent mechanisms leading to resistance to PDK1 inhibitors. Biochem. J. **448**:285-295.

43. **Zhou X, Cordon-Barris L, Zurashvili T, Bayascas JR.** 2014. Fine-tuning the intensity of the PKB/Akt signal enables diverse physiological responses. Cell Cycle **13**:3164-3168.

44. **Hauge C, Antal TL, Hirschberg D, Doehn U, Thorup K, Idrissova L, Hansen K, Jensen ON, Jorgensen TJ, Biondi RM, Frodin M.** 2007. Mechanism for activation of the growth factor-activated AGC kinases by turn motif phosphorylation. EMBO J. **26**:2251-2261.

45. **Le Good JA, Ziegler WH, Parekh DB, Alessi DR, Cohen P, Parker PJ.** 1998. Protein kinase C isotypes controlled by phosphoinositide 3-kinase through the protein kinase PDK1. Science **281**:2042-2045.

46. **Dutil EM, Toker A, Newton AC.** 1998. Regulation of conventional protein kinase C isozymes by phosphoinositide-dependent kinase 1 (PDK-1). Curr. Biol. **8**:1366-1375.

47. **Datta SR, Brunet A, Greenberg ME.** 1999. Cellular survival: a play in three Akts. Genes Dev. **13**:2905-2927.

48. **Yoshimura T, Arimura N, Kawano Y, Kawabata S, Wang S, Kaibuchi K.** 2006. Ras regulates neuronal polarity via the PI3-kinase/Akt/GSK-3beta/CRMP-2 pathway. Biochem. Biophys. Res. Commun. **340**:62-68.

49. **Kishi M, Pan YA, Crump JG, Sanes JR.** 2005. Mammalian SAD kinases are required for neuronal polarization. Science **307**:929-932.

50. **Barnes AP, Lilley BN, Pan YA, Plummer LJ, Powell AW, Raines AN, Sanes JR, Polleux F.** 2007. LKB1 and SAD kinases define a pathway required for the polarization of cortical neurons. Cell **129**:549-563.

51. **Laguesse S, Creppe C, Nedialkova DD, Prevot PP, Borgs L, Huysseune S, Franco B, Duysens G, Krusy N, Lee G, Thelen N, Thiry M, Close P, Chariot A, Malgrange B, Leidel SA, Godin JD, Nguyen L.** 2015. A Dynamic Unfolded Protein Response Contributes to the Control of Cortical Neurogenesis. Dev. Cell **35**:553-567.

52. **Creppe C, Malinouskaya L, Volvert ML, Gillard M, Close P, Malaise O, Laguesse S, Cornez I, Rahmouni S, Ormenese S, Belachew S, Malgrange B, Chapelle JP, Siebenlist U, Moonen G, Chariot A, Nguyen L.** 2009. Elongator controls the migration and differentiation of cortical neurons through acetylation of alpha-tubulin. Cell **136**:551-564.

53. **Holz MK, Ballif BA, Gygi SP, Blenis J.** 2005. mTOR and S6K1 mediate assembly of the translation preinitiation complex through dynamic protein interchange and ordered phosphorylation events. Cell **123**:569-580.

54. **Magnuson B, Ekim B, Fingar DC.** 2012. Regulation and function of ribosomal protein S6 kinase (S6K) within mTOR signalling networks. Biochem. J. **441**:1-21.

55. **Selemon LD, Goldman-Rakic PS.** 1999. The reduced neuropil hypothesis: a circuit based model of schizophrenia. Biol. Psychiatry **45**:17-25.

56. **Selemon LD, Rajkowska G, Goldman-Rakic PS.** 1998. Elevated neuronal density in prefrontal area 46 in brains from schizophrenic patients: application of a three-dimensional, stereologic counting method. J. Comp Neurol. **392**:402-412.

57. **Akbarian S, Huang HS.** 2006. Molecular and cellular mechanisms of altered GAD1/GAD67 expression in schizophrenia and related disorders. Brain Res. Rev. **52**:293-304.

58. **Lewis DA, Curley AA, Glausier JR, Volk DW.** 2012. Cortical parvalbumin interneurons and cognitive dysfunction in schizophrenia. Trends Neurosci. **35**:57-67.

59. **Miyamoto Y, Nitta A.** 2014. Behavioral Phenotypes for Negative Symptoms in Animal Models of Schizophrenia. J. Pharmacol. Sci.

60. **Stefansson H, Sigurdsson E, Steinthorsdottir V, Bjornsdottir S, Sigmundsson T, Ghosh S, Brynjolfsson J, Gunnarsdottir S, Ivarsson O, Chou TT, Hjaltason O, Birgisdottir B, Jonsson H, Gudnadottir VG, Gudmundsdottir E, Bjornsson A, Ingvarsson B, Ingason A, Sigfusson S, Hardardottir H, Harvey RP, Lai D, Zhou M, Brunner D, Mutel V, Gonzalo A, Lemke G, Sainz J, Johannesson G, Andresson T, Gudbjartsson D, Manolescu A, Frigge ML, Gurney ME, Kong A, Gulcher JR, Petursson H, Stefansson K.** 2002. Neuregulin 1 and susceptibility to schizophrenia. Am. J. Hum. Genet. **71**:877-892.

61. **Tosato S, Dazzan P, Collier D.** 2005. Association between the neuregulin 1 gene and schizophrenia: a systematic review. Schizophr. Bull. **31**:613-617.

Figure Legends.

FIG 1. Generation of brain-specific PDK1 L155E mice. (A) Diagram depicting the 5'-end of the PDK1 gene from exons 2 to 7 (PDK1); the targeting construct containing the thymidine kinase (TK) negative selectable marker and the minigene cassette, which includes the PDK1 open reading frame from exons 3 to 14 plus the natural polyadenylation signals (A^+), and is flanked by LoxP sites (CONSTRUCT); the targeted allele, which drives the expression of the PDK1 wild type protein in control tissues (PDK1 WT), and the excised allele in which the CRE-Recombinase mediated deletion of the minigene cassette allows the expression of the PDK1 mutant protein (PDK1 L155E). The white boxes represent exons, the black triangles represent LoxP sites, and the mutated exon four containing the Leu155Glu amino acid substitution is black–filled and labeled with an asterisk. (B) Breeding strategy used for the generation of mice expressing the PDK1 L155E mutant protein in brain. The number (n) and proportion (%) of mice of each genotype resulting from the depicted experimental breeding are indicated both at embryonic day 15.5 (E15) and at birth (P0). ** indicates that the lower-than-expected frequency of $PDK1^{fl/fl}$ CRE^+ pups is statistically significant ($P < 0.005$ by χ^2 test). (C) PDK1 was affinity purified on PIF-sepharose from liver or brain embryonic extracts of the indicated genotypes. The expression levels of the PDK1 wild type protein were quantified on the indicated genotypes and tissues from the PDK1 immunoblot signals of the PIF-Sepharose pulldowns (middle panels), normalized by the total PDK1 protein levels derived from the whole tissue lysate immunoblot signals (upper panels), and represented as percentage of the $PDK1^{+/fl}$ CRE^- controls. Each bar represents the means ± standard errors of the mean for the immunoblot signals derived from two independent experiments. A representative western blot is shown,

878 where each lane corresponds to a sample derived from a different mice. Immunoblots with
879 the ERK1/2 antibody are also shown as control of protein loading (bottom panels).
880
881 **FIG 2.** Microcephaly of the PDK1$^{fl/fl}$ CRE^{+} mice. The organ volume was measured from
882 physical histological sections of the E15,5 embryo head (A) and brain (C) or MRI-obtained
883 images of one hemisphere of the adult brain (D) by using the Cavalieri method as described
884 in Materials and Methods. The data are represented as the means ± standard errors of the
885 mean obtained for three different mice per genotype, and are expressed as percentage of the
886 controls. The total volume values and representative photographs of the E15,5 embryonic
887 brains or adult brain left hemispheres are shown at the bottom, where the scale bars
888 correspond to 1 mm and 2 mm, respectively. (B) The mean body weights of mice of the
889 indicated genotypes are shown. The values represent the means ± standard errors of the
890 mean for the indicated number of mice (n). (E and F) The number of cells (E) and the
891 cellular volume (F) were determined from E15.5 dissociated cortical neurons with a
892 Scepter^{TM} 2.0 Handheld Automated Cell Counter (Millipore). The data are represented as
893 the means ± standard errors of the means for the indicated number of embryos (n) obtained
894 from 11 independent litters.
895
896 **FIG 3.** Activation of S6K1, RSK, SGK1 and PKC, but not Akt, is inhibited in the PDK1$^{fl/fl}$
897 CRE^{+} mice. (A) Cortical neurons from three independent embryos of the indicated
898 genotypes were cultured for 6 DIV, then serum starved for 4 h and either left unstimulated
899 or stimulated with 50 ng/ml of BDNF for 15 minutes. (B) Whole brain protein extracts
900 were obtained at E15,5 from three independent embryos of each depicted genotype. Lysates
901 were immunoblotted with the indicated antibodies to monitor the activation of Akt, S6K,

902 RSK, SGK and PKC, were each lane corresponds to a different embryo. Band densitometry
903 quantification of the ratio between phosphorylated and total protein levels is shown at the
904 bottom, where bars represent the means ± standard errors of the mean obtained for the three
905 different mice per genotype analyzed, and are expressed as percentage of the BDNF-
906 stimulated control samples (A) or control brain tissue samples (B).
907
908 **FIG 4.** Neuronal survival responses are preserved in the PDK1$^{fl/fl}$ CRE^{+} mice. Cortical cells
909 of the indicated genotypes were either sham treated (CONTROL) or deprived of trophic
910 factors in the absence (TD) or presence of 50 ng/ml of BDNF (TD+BDNF) for 24 h. Data
911 represent the means ± standard errors of the means for at least 3 independent mouse
912 embryos per genotype from 6 independent litters. (A) Viability was determined with the
913 MTT reduction assay and is expressed as a percentage of the untreated cells. (B) The
914 percentage of apoptotic cells was obtained by scoring the number of nuclei exhibiting
915 chromatin fragmentation from six different fields per well and 4 wells per condition divided
916 by the total. (C) Representative micrographs of Hoechst-stained cortical neurons of the
917 indicated genotypes after 24 h of the indicated treatment; arrowheads indicate apoptotic
918 nuclei. Bar, 20 μm.
919
920 **FIG 5.** Reduced neuronal progenitor proliferation in the PDK1$^{fl/fl}$ CRE^{-} and PDK1$^{fl/fl}$ CRE^{+}
921 embryos. (A) Representative micrographs of E15,5 embryonic cortical cultures of the
922 indicated genotypes immunostained with the described antibodies. Bar, 40 μm. The
923 percentage of primary cortical neurons expressing the Ki67 proliferation marker (B) or the
924 active caspase-3 apoptotic marker (C) were scored at the indicated time points, were each
925 bar corresponds to the means ± standard errors of the means from ten different fields per

culture and three independent embryonic cultures per genotype. (D) Epifluorescence microscopy images of E15,5 embryonic brain coronal sections of the indicated genotypes immunostained with the described antibodies. Bar, 100 μm. The intensity of Doublecortin (DCX) staining (E) and the number of caspase-3 positive cells per field (F), were quantified and expressed as the mean ± standard error of the mean from three independent sections per embryo obtained from three different embryos per genotype.

FIG 6. Deficient polarization and axonal outgrowth in the PDK1$^{fl/fl}$ CRE^{-} and PDK1$^{fl/fl}$ CRE^{+} mice. (A) Representative micrographs of hippocampal cultures from the indicated genotypes at different days in vitro (DIV) stained with the dendrite-specific marker MAP2 (red) and the specific axonal marker Tau-1 (green). Bar, 50 μm. (B and D) The percentage of polarization (B), the number of neurites per cell (C), the diameter of the soma (D) and the length of neurites, neurites ramifications and axons (E), were measured at different time points on samples from the indicated genotypes. Each bar represents the mean ± standard error of the mean for 100 neurons from three different embryos per condition.

FIG 7. Reduced connectivity in the PDK1$^{fl/fl}$ CRE^{-} and PDK1$^{fl/fl}$ CRE^{+} mice brain. (A) Epifluorescence micrographs of coronal sections of the somatosensory cortex from mice brains of the indicated genotypes stained with the dendrite-specific marker MAP2, the general axonal marker SMI312, and the nuclear Hoechst dye. The merged signals are also shown. Cortical layers are depicted on the right from I to VI. Bar, 100 μm.

(B) Image magnifications of cortical layers IV and VI, as well as the hippocampal dentate girus (DG), CA3 and CA1 regions stained with SMI312 and Hoechst. Arrowheads indicate differences in the density of axonal fibers between genotypes. Bar, 50 μm.

FIG 8. Abnormal cortical layering with compactation of Layer IV in PDK1$^{fl/fl}$ CRE^{-} and PDK1$^{fl/fl}$ CRE^{+} mice brain. (A and C) Epifluorescence microscopy images of coronal sections of the somatosensory cortex from mice of the indicated genotypes stained with the neuronal marker NeuN and the nuclear Hoechst dye, as indicated. Adjacent hematoxylin-and-eosin (H-E)-stained sections and the merged signals are also shown. Bar, 100 μm. Cortical layers are indicated on the right from I to VI. A low magnification micrograph of the hematoxylin-and-eosin (H-E)-stained sections and a high magnification of the merged epifuorescence images corresponding to layers II to V are also shown at the top of each panel.

FIG 9. Reduced GAD67 levels and abnormal parvalbumin-staining patterns in the PDK1$^{fl/fl}$ CRE^{-} and PDK1$^{fl/fl}$ CRE^{+} mice brain. (A and B) Epifluorescence microscopy images of coronal sections of the somatosensory cortex from mice of the indicated genotypes stained with the layer II to IV-specific marker CUX1, the gabaergic neuron-specific marker GAD67, the interneuron marker parbalvumin, and the nuclear Hoechst dye, as indicated. Cortical layers are indicated on the right from I to VI. Bar, 100 μm. (C and E) The density of neurons in layer IV (C), the percentage of CUX1-positive neurons in layer IV among the total number of CUX1-positive neurons in layers I to IV (D), and the intensity of GAD67 staining (E), were quantified and expressed as the mean ± standard error of the mean from three independent sections per embryo obtained from three different embryos per genotype.

970 (F) Epifluorescence microscopy images of coronal sections of the cingulated cortex from
971 mice of the indicated genotypes stained with the the gabaergic neuron-specific marker
972 GAD67 and the nuclear Hoechst dye. Higher magnification images of layer II-III (a) and
973 layer V (b) regions are also shown. Bar, 200 μm.
974
975 **FIG 10.** Disruptive behavior with diminished motivation and cognitive deficits in the
976 $PDK1^{fl/fl}$ CRE^{+} mice. (A and H) The somatic growth–related parameters (A), the
977 sensorimotor performance on the wood rod test (B), the executive functions in the nesting
978 behavior daily life activity (C), the incidence of bizarre behaviors (D), the exploratory
979 activity and anxiety-like behaviors in a standard open-field test (E), the level of interaction
980 in the marble-burying test (F), the cognitive abilities in the water maze and depression-like
981 diminished motivation measured by episodes of immobility (G) and the circadian activity
982 on running wheels (H) were assessed on six $PDK1^{fl/fl}$ CRE^{-} (WT, black bars and dots) and
983 six $PDK1^{fl/fl}$ CRE^{+} (L155E, white bars and dots) adult female mice.

CORDON-BARRIS_FIG1

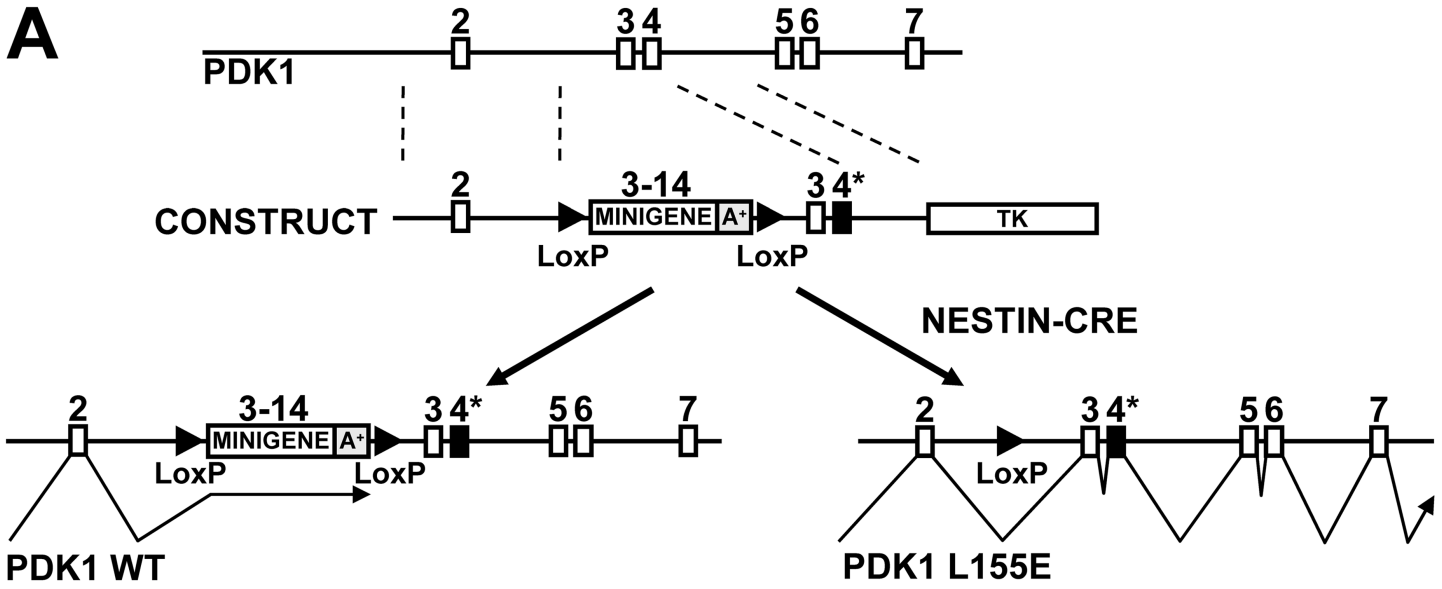

B

PDK1 $^{+/fl}$ CRE+ x PDK1 $^{fl/fl}$ CRE-

	E 15.5		P 0	
	n	(%)	n	(%)
PDK1 $^{+/fl}$ CRE-	45	28,1	79	32,4
PDK1 $^{+/fl}$ CRE+	48	28,1	83	34,0
PDK1 $^{fl/fl}$ CRE-	35	23,6	63	25,8
PDK1 $^{fl/fl}$ CRE+	31	20,2	19	7,8**

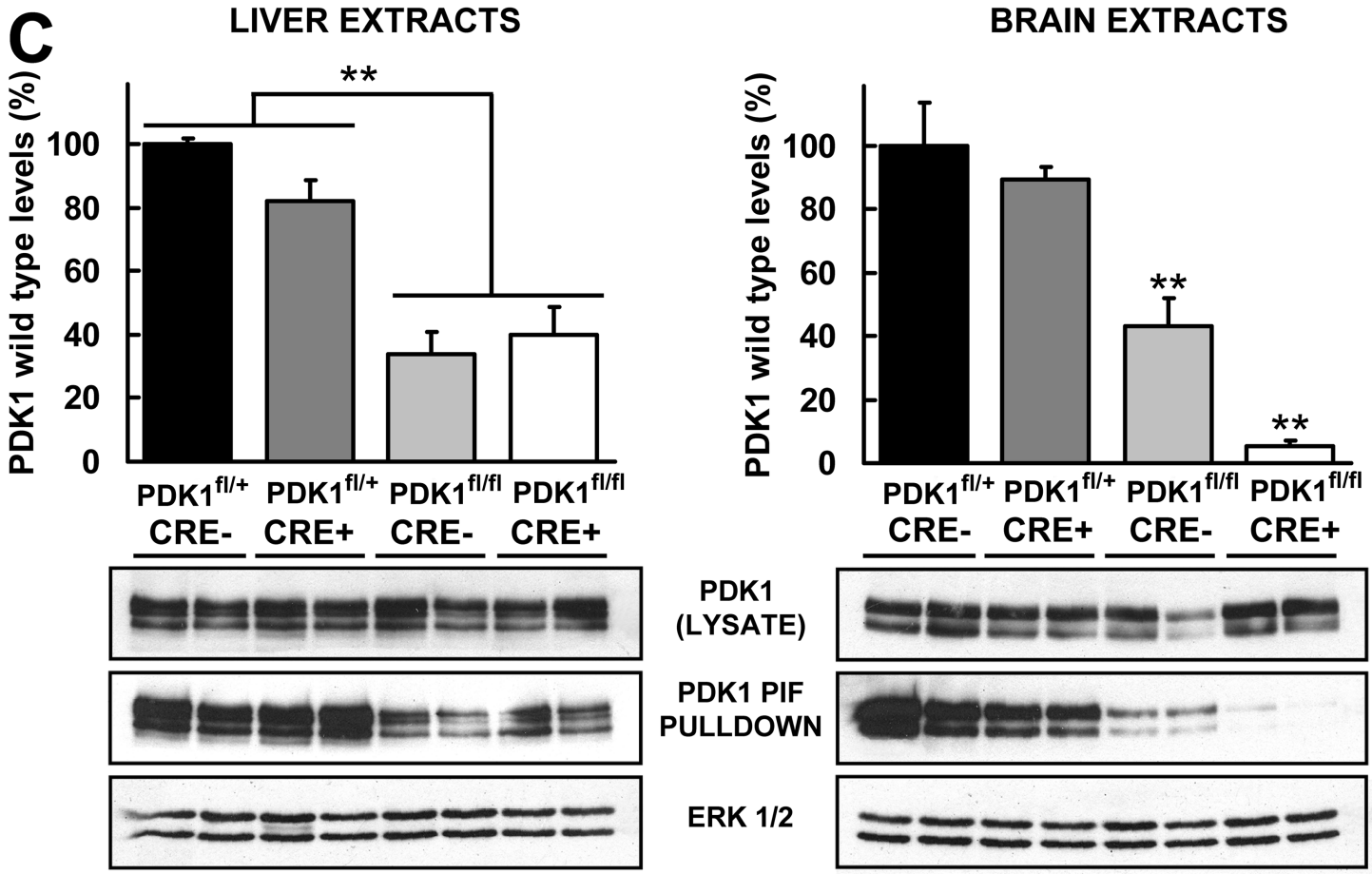

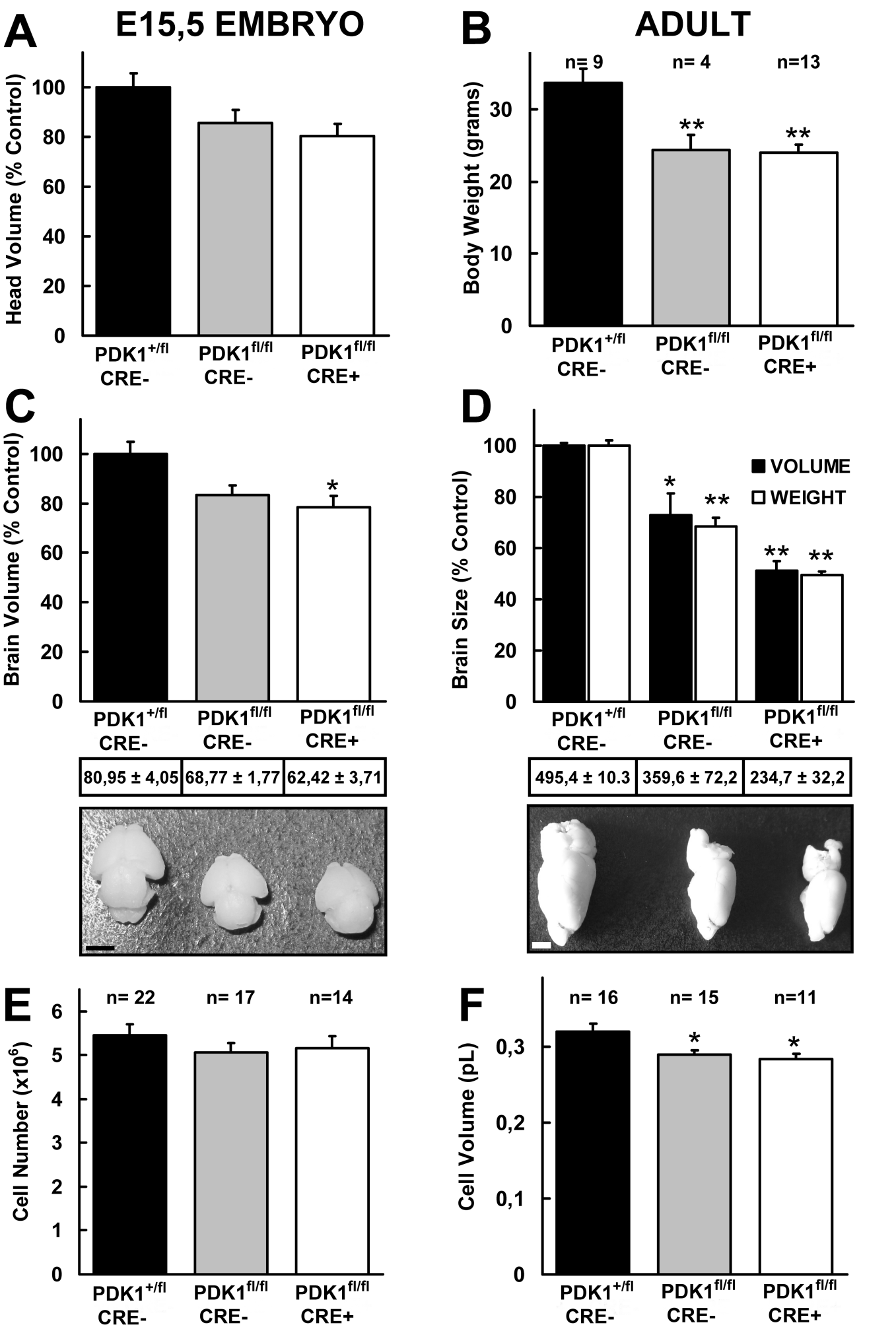
A
E15,5 EMBRYO
Head Volume (% Control)
100
80
60
40
20
0
PDK1+/fl CRE-
PDK1fl/fl CRE-
PDK1fl/fl CRE+
B
ADULT
n= 9
n= 4
n=13
Body Weight (grams)
30
20
10
0
**
**
PDK1+/fl CRE-
PDK1fl/fl CRE-
PDK1fl/fl CRE+
C
Brain Volume (% Control)
100
80
60
40
20
0
*
PDK1+/fl CRE-
PDK1fl/fl CRE-
PDK1fl/fl CRE+
80,95 ± 4,05
68,77 ± 1,77
62,42 ± 3,71
D
Brain Size (% Control)
100
80
60
40
20
0
VOLUME
WEIGHT
*
**
**
**
PDK1+/fl CRE-
PDK1fl/fl CRE-
PDK1fl/fl CRE+
495,4 ± 10.3
359,6 ± 72,2
234,7 ± 32,2
E
n= 22
n= 17
n=14
Cell Number (x10^6)
6
5
4
3
2
1
0
PDK1+/fl CRE-
PDK1fl/fl CRE-
PDK1fl/fl CRE+
F
n= 16
n= 15
n=11
Cell Volume (pL)
0,3
0,2
0,1
0
*
*
PDK1+/fl CRE-
PDK1fl/fl CRE-
PDK1fl/fl CRE+

CORDON-BARRIS_FIG3

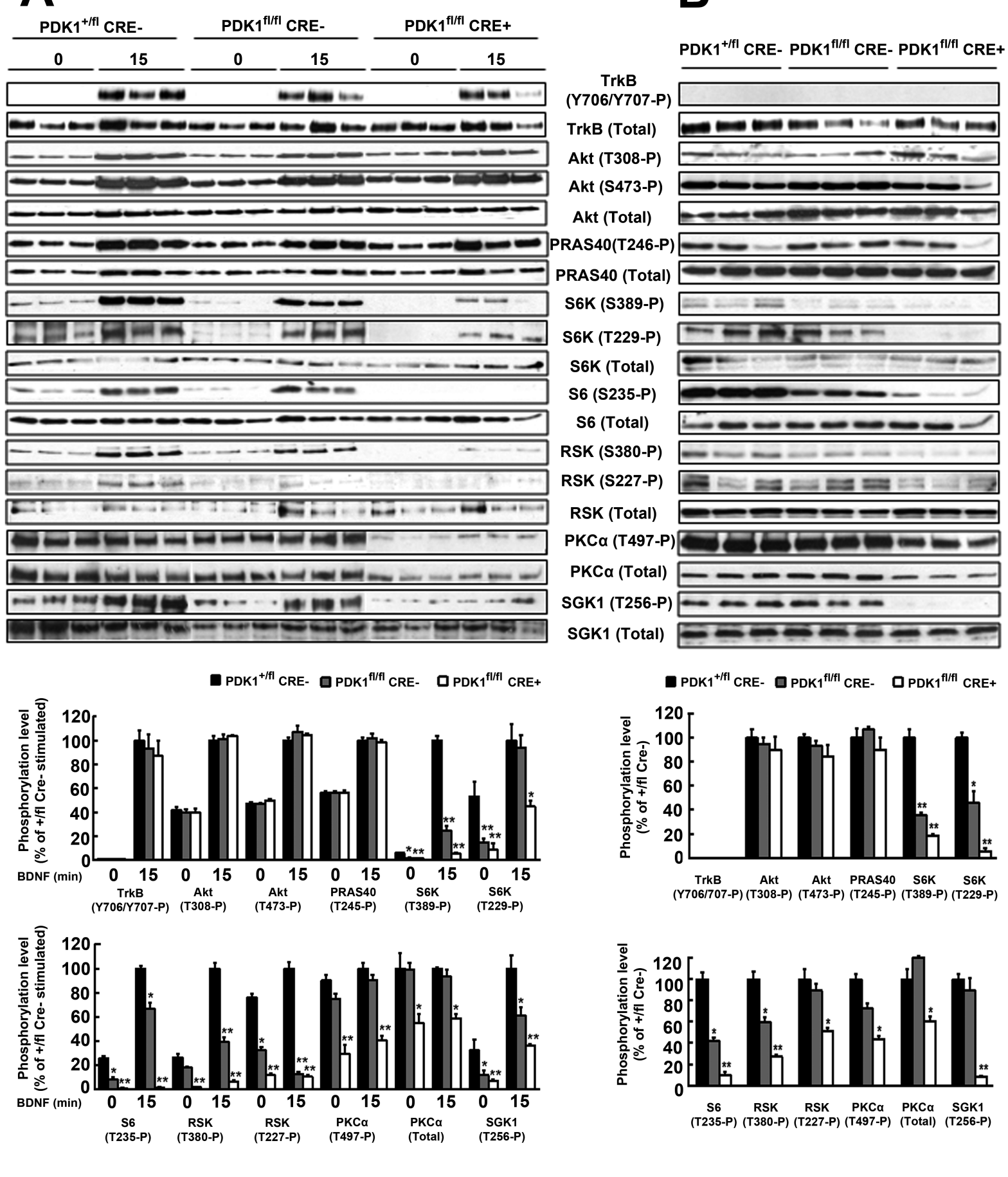

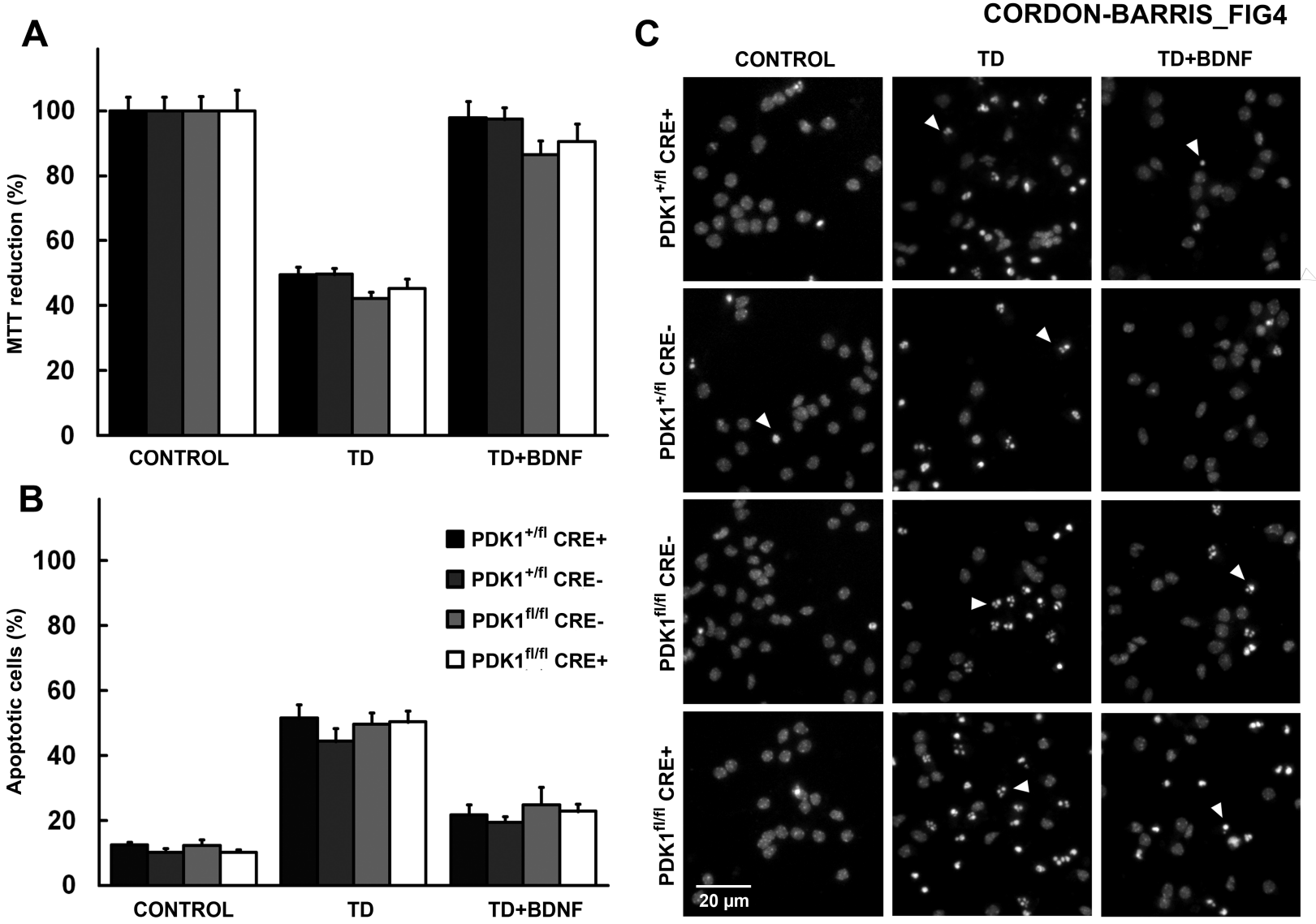
CORDON-BARRIS_FIG4
A
MTT reduction (%)
100
80
60
40
20
0
CONTROL
TD
TD+BDNF
B
Apoptotic cells (%)
100
80
60
40
20
0
PDK1+/fl CRE+
PDK1+/fl CRE-
PDK1fl/fl CRE-
PDK1fl/fl CRE+
CONTROL
TD
TD+BDNF
C
CONTROL
TD
TD+BDNF
PDK1+/fl CRE+
PDK1+/fl CRE-
PDK1fl/fl CRE-
PDK1fl/fl CRE+
20 µm

CORDON-BARRIS_FIG5

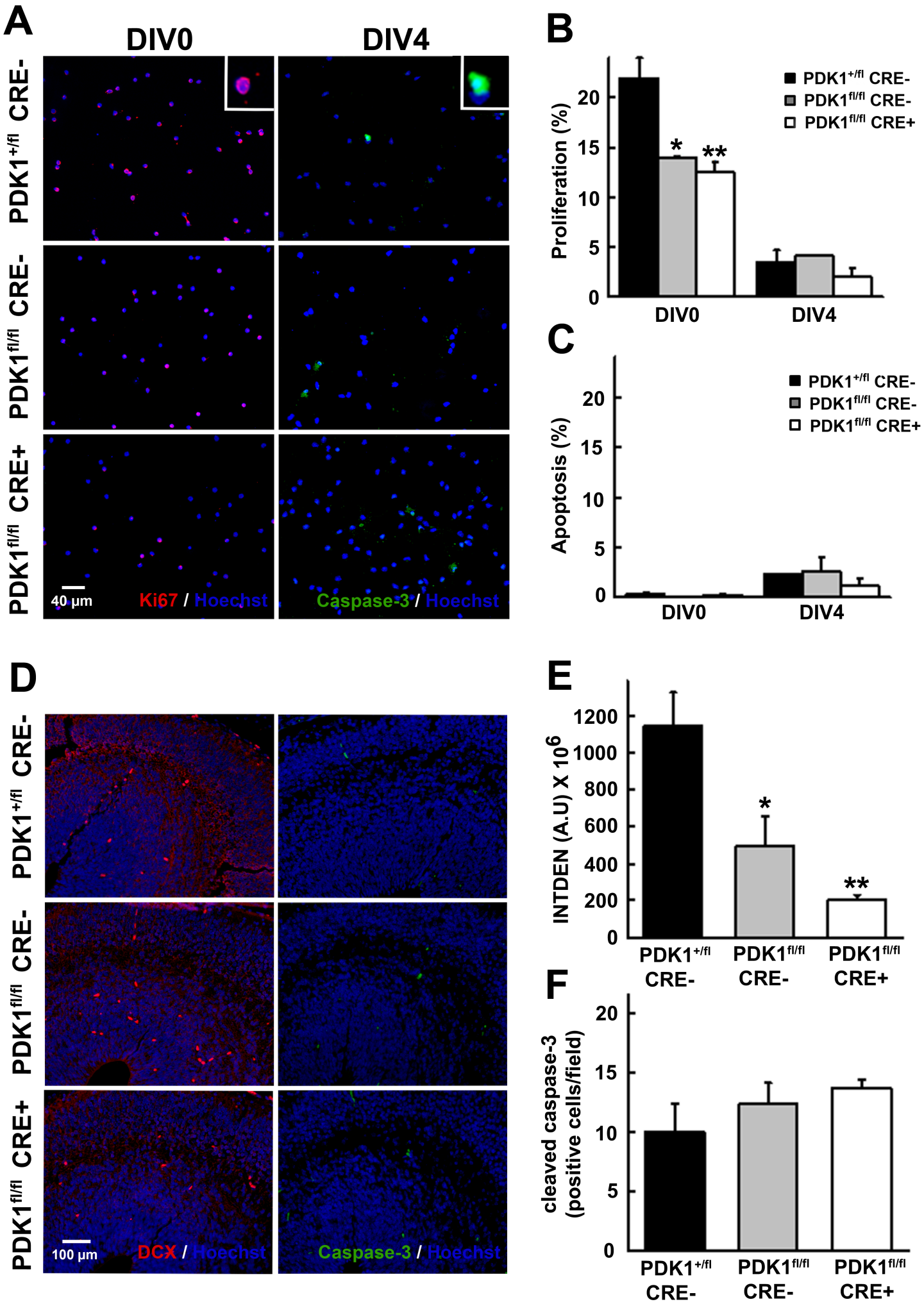

CORDON-BARRIS_FIG6

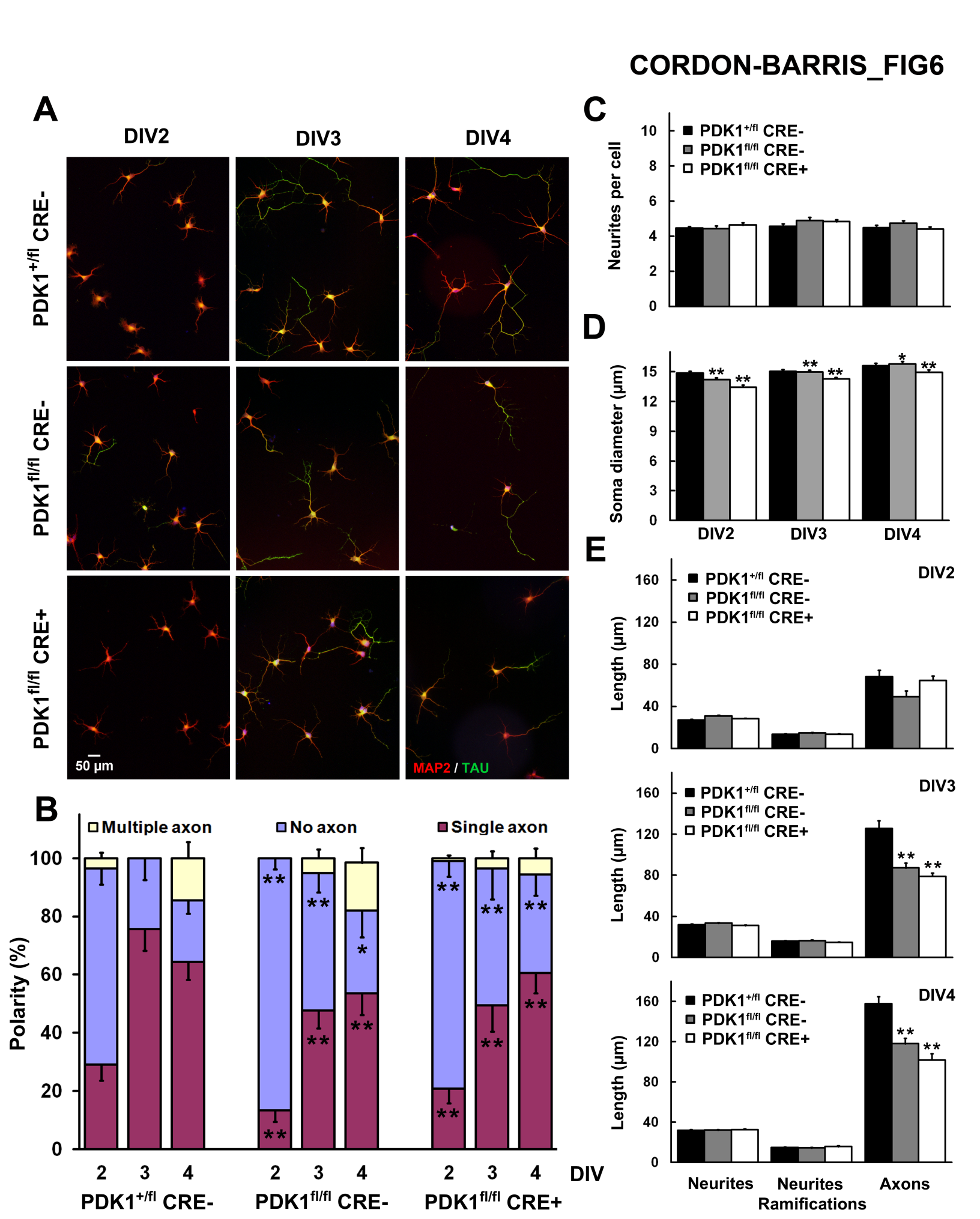

CORDON-BARRIS_FIG7

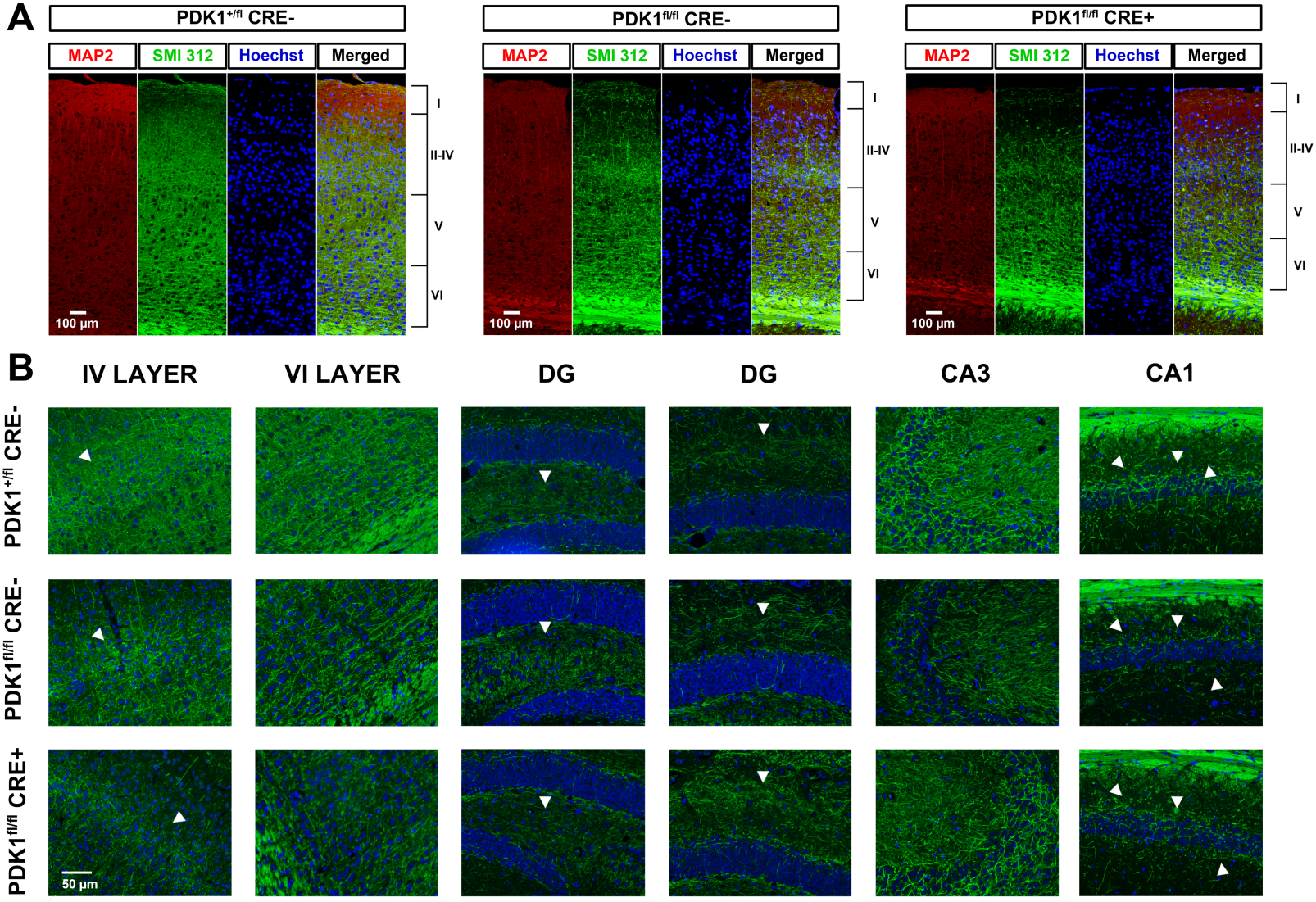

CORDON-BARRIS_FIG8

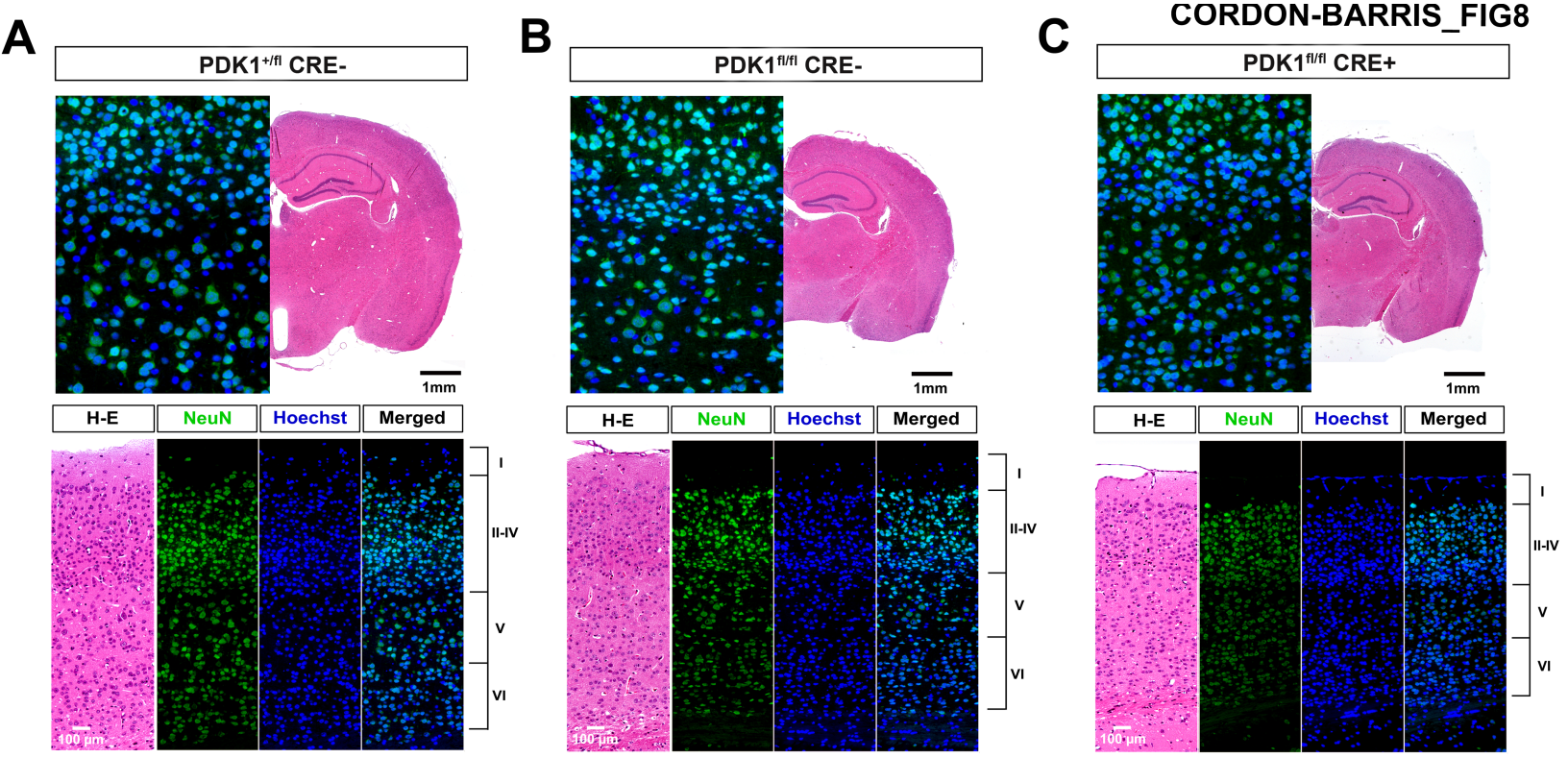

CORDON-BARRIS_FIG9

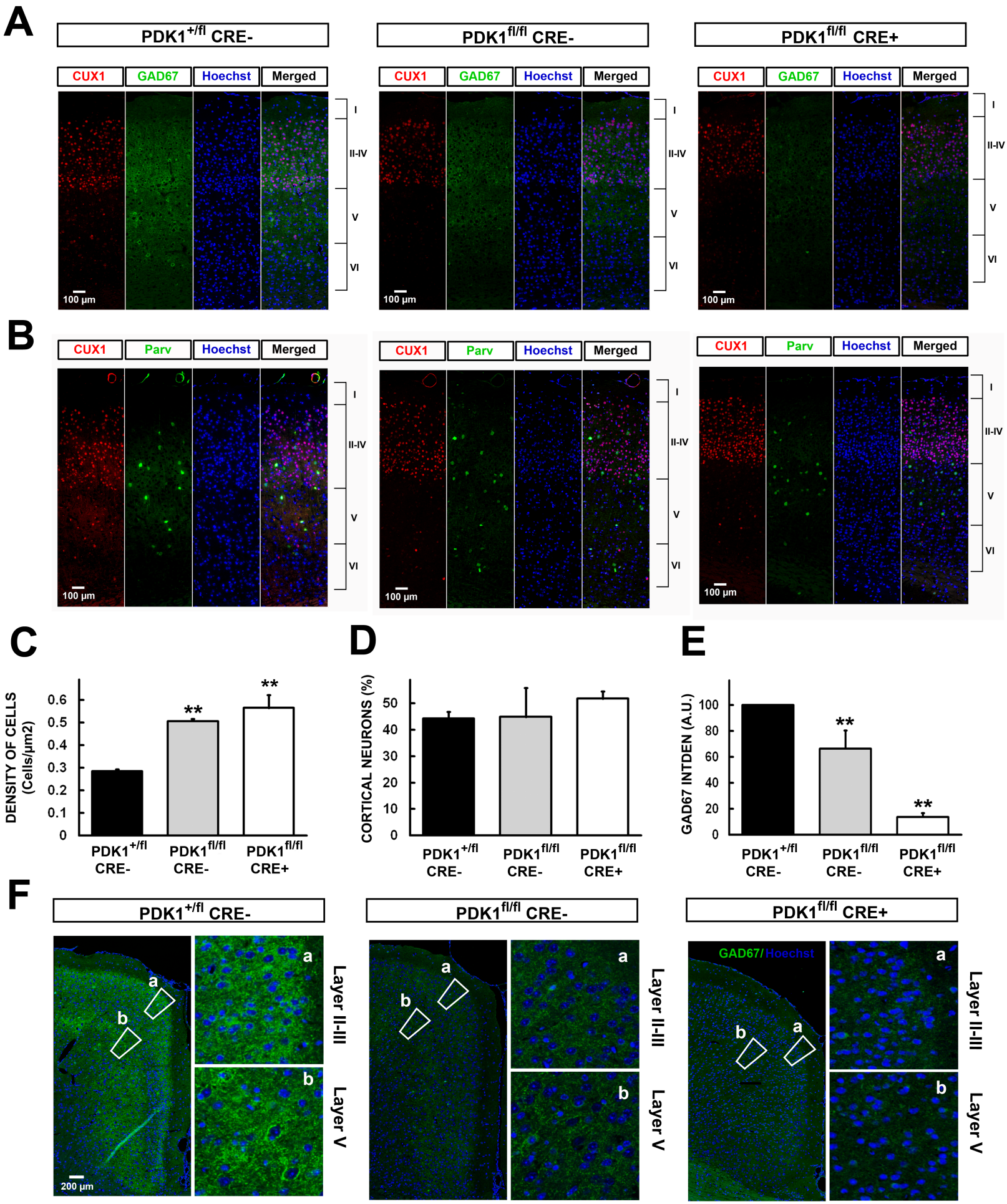

CORDON-BARRIS_FIG10